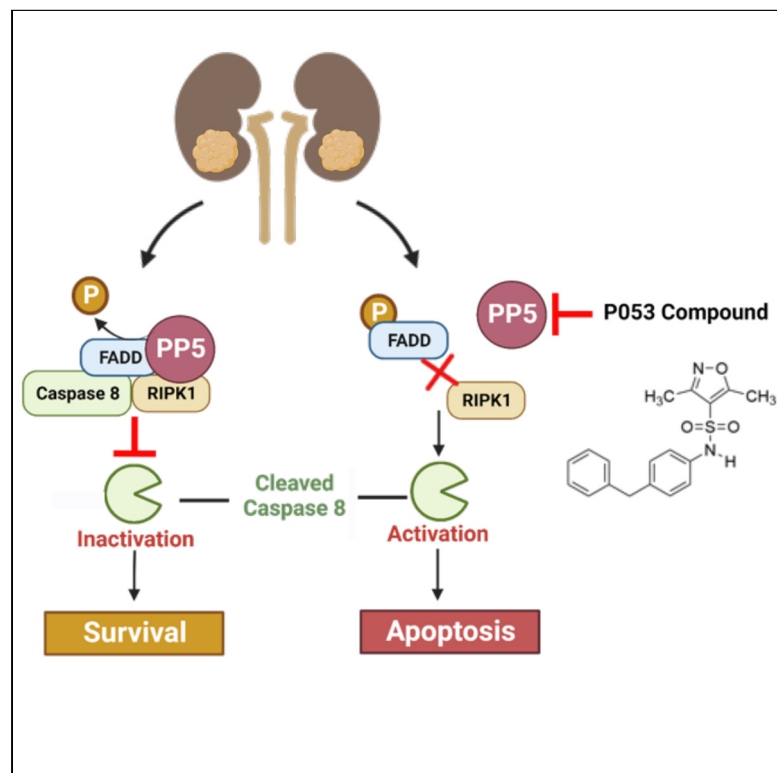


Cell Chemical Biology

Catalytic inhibitor of Protein Phosphatase 5 activates the extrinsic apoptotic pathway by disrupting complex II in kidney cancer

Graphical abstract



Authors

Elham F. Ahanin, Rebecca A. Sager, Sarah J. Backe, ..., Dimitra Bourboulia, John D. Chisholm, Mehdi Mollapour

Correspondence

bourmpod@upstate.edu (D.B.),
jdchisho@syr.edu (J.D.C.),
mollapom@upstate.edu (M.M.)

In brief

Ahanin et al. show that protein phosphatase-5 (PP5) down-regulates the extrinsic apoptotic pathway by dephosphorylating the death effector protein FADD, therefore preserving complex II integrity in cancer. A competitive inhibitor of PP5 designed in this study causes disruption of complex II and activation of extrinsic apoptotic pathway in renal cancer.

Highlights

- PP5 mediates dephosphorylation and inactivation of the death effector protein FADD
- PP5 maintains the integrity of complex II and regulates the extrinsic apoptosis
- Development of competitive inhibitors of serine/threonine protein phosphatase-5
- Pharmacologic inhibition of PP5 activates the extrinsic apoptosis in renal cancer

Article

Catalytic inhibitor of Protein Phosphatase 5 activates the extrinsic apoptotic pathway by disrupting complex II in kidney cancer

Elham F. Ahanin,^{1,2,3} Rebecca A. Sager,^{1,3} Sarah J. Backe,^{1,3} Diana M. Dunn,^{1,2,11} Natela Dushukyan,^{1,2,3} Adam R. Blanden,⁴ Nilamber A. Mate,⁵ Tamie Suzuki,⁵ Tyler Anderson,^{1,6} Merin Roy,^{1,2,3} Jasmeen Oberoi,⁷ Chrisostomos Prodromou,⁸ Imad Nsouli,^{1,3} Michael Daneshvar,⁹ Gennady Bratslavsky,^{1,2,3} Mark R. Woodford,^{1,2,3} Dimitra Bourboulia,^{1,2,3,*} John D. Chisholm,^{5,*} and Mehdi Mollapour^{1,2,3,10,12,*}

¹Department of Urology, SUNY Upstate Medical University, Syracuse, NY 13210, USA

²Department of Biochemistry and Molecular Biology, SUNY Upstate Medical University, Syracuse, NY 13210, USA

³Upstate Cancer Center, SUNY Upstate Medical University, Syracuse, NY 13210, USA

⁴Department of Neurology, SUNY Upstate Medical University, Syracuse, NY 13210, USA

⁵Department of Chemistry, Syracuse University, Syracuse, NY 13210, USA

⁶College of Health Professions, SUNY Upstate Medical University, Syracuse, NY 13210, USA

⁷Genome Damage and Stability Centre, School of Life Sciences, University of Sussex, Brighton BN1 9RQ, UK

⁸School of Life Sciences, Biochemistry and Biomedicine, University of Sussex, Falmer, Brighton BN1 9QG, UK

⁹Department of Urology, University of California, California, Irvine, CA 92868, USA

¹⁰Twitter: @medmol

¹¹Present address: Department of Biochemistry and Biophysics, School of Medicine and Dentistry, University of Rochester, Rochester, NY

¹²Lead contact

*Correspondence: bournpod@upstate.edu (D.B.), jdchisho@syr.edu (J.D.C.), mollapom@upstate.edu (M.M.)

<https://doi.org/10.1016/j.chembiol.2023.06.026>

SUMMARY

Serine/threonine protein phosphatase-5 (PP5) is involved in tumor progression and survival, making it an attractive therapeutic target. Specific inhibition of protein phosphatases has remained challenging because of their conserved catalytic sites. PP5 contains its regulatory domains within a single polypeptide chain, making it a more desirable target. Here we used an *in silico* approach to screen and develop a selective inhibitor of PP5. Compound P053 is a competitive inhibitor of PP5 that binds to its catalytic domain and causes apoptosis in renal cancer. We further demonstrated that PP5 interacts with FADD, RIPK1, and caspase 8, components of the extrinsic apoptotic pathway complex II. Specifically, PP5 dephosphorylates and inactivates the death effector protein FADD, preserving complex II integrity and regulating extrinsic apoptosis. Our data suggests that PP5 promotes renal cancer survival by suppressing the extrinsic apoptotic pathway. Pharmacologic inhibition of PP5 activates this pathway, presenting a viable therapeutic strategy for renal cancer.

INTRODUCTION

The serine/threonine protein phosphatase PP5 regulates several signaling cascades that are responsible for tumor initiation, progression, and metastasis.^{1–3} Unlike other family members, a single gene encodes PP5, and its regulatory and catalytic domains are all contained within the same polypeptide.^{4–9} PP5 generally has low basal activity due to the interaction of the tetratricopeptide repeat (TPR) motif at its amino-terminus with the α J-helix in the carboxy-terminus. This autoinhibitory state prevents substrates from entering the active site of PP5.^{10–14} Additionally, PP5 is a co-chaperone of the molecular chaperone heat shock protein-90 (Hsp90). Binding of PP5 TPR domain to Hsp90 releases its autoinhibition and activates PP5.^{11,14–16} Other cellular factors such as polyunsaturated fatty acids have also been described to activate PP5 *in vitro*.^{13,14,17} Furthermore, we have

shown that post-translational modifications of PP5 play a major role in its switching “on” and “off” in cells.² The Von Hippel-Lindau (*VHL*) tumor suppressor gene is the recognition subunit of an E3 ubiquitin ligase that canonically recognizes its substrates following an oxygen-dependent prolyl-hydroxylase (PHD) reaction, with hypoxia-inducible factor (HIF α) being its most-studied substrate.^{18–20} However, previous studies, including from our group, have demonstrated an oxygen and PHD-independent function for VHL.^{2,21–23} VHL is involved in multi-monoubiquitination and subsequent proteasomal degradation of PP5 in a hypoxia- and prolyl-hydroxylation-independent manner in normal cells therefore providing an “off” switch for PP5. The most common type of kidney cancer, clear cell renal cell carcinoma (ccRCC), is closely associated with mutations and inactivation of the *VHL* tumor suppressor gene.^{24–26} We have previously shown that *VHL*-deficient renal cancer cell lines

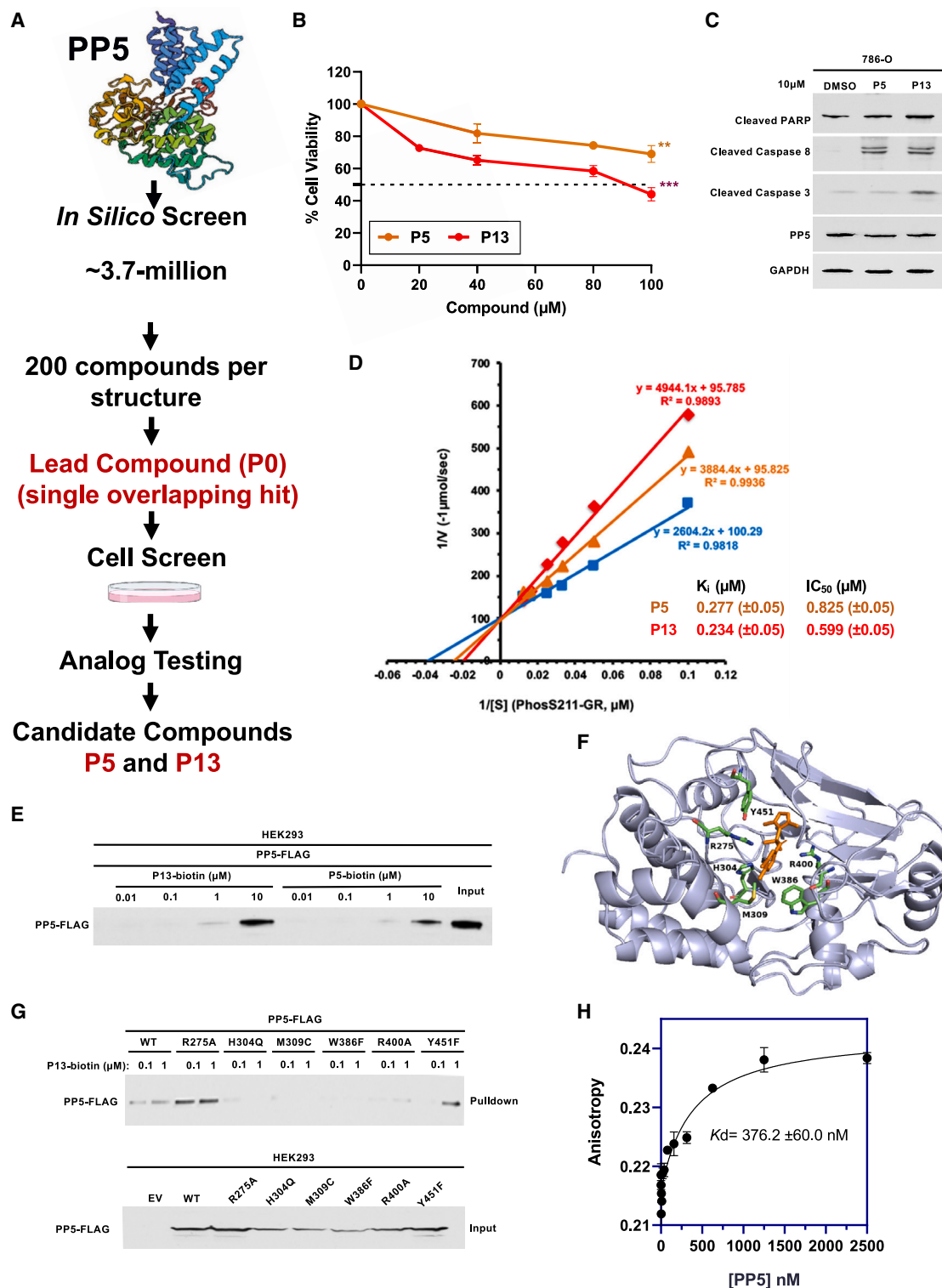


Figure 1. Identification and characterization of small molecule inhibitors of PP5

(A) Schematic workflow of *in silico* screening a library of ~3.7-million compounds to identify potential PP5 inhibitors. A single overlapping hit, P0 was used to identify a set of analogs for cell-based screening. Compounds 5 (P5) and 13 (P13) were selected as candidate PP5 inhibitors.

(B) 786-O cells were treated with the indicated amounts of P5 and P13 for 48 h. The effect of PP5 inhibitors on cell viability was assessed by MTT assay. Error bars represent the standard deviation (S.D.) of three independent experiments. A Student's *t* test was performed to assess statistical significance ***p* < 0.01; ****p* < 0.001.

(legend continued on next page)

and patient-derived ccRCC tumors exhibit elevated PP5 levels.² Additionally, casein kinase 1 δ (CK1 δ)-mediated phosphorylation of T362 in the catalytic domain of PP5 activates this phosphatase.² Pharmacological inhibition of CK1 δ or down-regulation of PP5 induced apoptosis and reduced proliferation in *VHL*-null ccRCC cells, suggesting a prosurvival role for PP5 in kidney cancer.² The mechanism of PP5-dependent cell survival and whether PP5 can be directly targeted, however, remains elusive.

In this study we used *in silico* structure-based drug discovery approach and identified a small molecule (P053) that specifically binds and inhibits PP5 activity. Inhibition of PP5 in *VHL*-null ccRCC cells leads to induction of the extrinsic apoptotic pathway. We found that PP5 interacts with the extrinsic apoptotic complex II members FADD, RIPK1, and caspase 8 and dephosphorylates S194-FADD in an Hsp90 independent manner. Inhibition or down-regulation of PP5 leads to disassociation of this complex, cleavage of caspase 8, and activation of the extrinsic apoptotic pathway in ccRCC.

RESULTS

Characterization of PP5 specific inhibitors

Since PP5 plays a major role in survival of ccRCC, we sought to design, develop, and test specific small molecule inhibitors of this phosphatase.³ In order to identify small molecule antagonists of PP5 an *in silico* docking study was initiated using our previously solved X-ray crystal structure of the PP5 active site (PDB:5HPE).⁶ The PP5 structure allowed us to employ a virtual screening strategy to identify new inhibitors of PP5 (Figure 1A). Docking was performed three times with three different structures, the only differences in the X-ray structures being the nature of the metal ion bound in the active site; Mn²⁺ for PDB: 3H60, Zn²⁺ for PDB:3H68 and Fe²⁺ was substituted for the Zn²⁺ ion in the PDB:3H68 structure²⁷ (Figures 1A and S1A). The 3-fold docking was performed due to the promiscuity of PP5 when it comes to metal ion in the active site, which can be Zn, Mn, or Fe based. The active site residues of D271, N303, H304, M309, and W386 were chosen to define the site for docking. Conducting a virtual screen with the Zinc library of drug like compounds (~3.7 million compounds)^{28,29} and DOCK Blaster³⁰ provided a set of 200 compounds for each crystal structure that were predicted to bind to the active site of PP5. Interestingly, only one compound (P0) was found to overlap between two of these hit-sets (Mn²⁺ and Zn²⁺) despite the significant similarity in the crystal structures (Figure S1B).

We first treated the ccRCC cell line 786-O with the overlapping hit compound P0 and showed a dose-dependent increase in phosphorylation of the known PP5 substrates phospho-S13-Cdc37 and phospho-S211-GR (Figure S1C). This suggested inhibition of PP5-mediated dephosphorylation of these known substrates. Based on the structure of P0, a number of similar molecules were purchased and assayed (Figure S1D, compounds P1-P13) to determine which section of the molecule contained the pharmacophore. 786-O cells were treated with 20 μ M compounds P0-P13 for 18 h, and induction of apoptosis and inhibition of PP5 was assessed by immunoblotting (Figure S1E). Compounds P4 to P13 led to marked increases in cleaved caspase-3 (indication of apoptosis) and elevated phosphorylation of PP5 substrates phospho-S13-Cdc37 and phospho-S211-GR (indication of PP5 inhibition) (Figure S1E). We next examined the effect of varying doses of compounds P4 to P13 on proliferation of ccRCC cells by the 3-(4, 5-dimethylthiazolyl)-2, 5-diphenyltetrazolium bromide (MTT) assay (Figure S1F). Compounds P5 and P13 significantly inhibited the proliferation of 786-O cells (Figure 1B) and were therefore selected for further evaluation. These compounds were resynthesized and their structures were confirmed by ¹H NMR, ¹³C NMR and high-resolution mass spectrometry (Figures S2A–S2D). We further examined the effect of P5 and P13 on 786-O cells by immunoblotting and demonstrate cleavage of the apoptotic markers caspase-3 and 8 and PARP (Figure 1C). Taken together, we have identified two potential PP5 small molecule inhibitors that led to induction of apoptosis in ccRCC cells.

PP5 inhibitors specifically bind to the phosphatase-catalytic domain

We next sought to measure the inhibition of PP5 activity *in vitro* with P5 and P13. This was done using custom synthesized phospho-S211-glucocorticoid receptor (GR) peptide as a specific substrate and measuring PP5 activity by assessing free phosphate release as a result of PP5-mediated peptide dephosphorylation. As expected, our enzyme kinetics confirmed P5 and P13 to be competitive inhibitors of PP5 (Figure 1D) with K_i of P5 = 277 \pm 50 nM and P13 = 234 \pm 50 nM. The binding data are summarized in Figure 1D. To obtain further evidence to support the binding of P5 and P13 compounds to PP5 *in vivo*, we synthesized biotinylated-P5 and biotinylated-P13 (Figures S2E and S2F). For compound P5, this was accomplished by hydrolysis of the ester on P5, amide formation with a piperazine linker, and attachment of biotin to the distal piperazine nitrogen (Figure S2E). In the case of compound P13, an aminopropyl linker was added to the sulfonamide nitrogen, with biotin then being attached to the far end of the linker (Figure S2F). We next transiently expressed PP5-FLAG in HEK293 cells and then challenged the protein lysate

(C) 786-O cells were treated with 10 μ M P5 or P13 or DMSO vehicle control for 24 h. Induction of apoptosis was assessed by immunoblotting. GAPDH was used as a loading control.

(D) PP5 enzyme kinetic data with P5 (orange line), P13 (red line) or no inhibitor (blue line) presented as a Lineweaver–Burk plot (n = 3 independent samples).

(E) Lysates from HEK293 cells transfected with PP5-FLAG were incubated with indicated amounts of biotin-labeled P5 and P13 followed by streptavidin agarose pulldown. Co-pulldown of PP5-FLAG was detected by immunoblotting.

(F) Crystal structure of PP5 active site (gray; PDB: 3H60) with predicted residues responsible (green) for contact with P13 (orange) modeled with PyMOL software (v4.6.0).

(G) WT-PP5-FLAG and predicted binding residue mutants were transiently expressed in HEK293 cells. Lysate was incubated with indicated amounts of biotinylated P13 followed by streptavidin pulldown (above). PP5 binding to biotinylated P13 was examined by immunoblot. Input expression of PP5-FLAG and mutants is below. EV was used as a control.

(H) P13-BODIPY binding to PP5 measured by fluorescence anisotropy. Points are replicate means \pm SEM from independent trials for display. (n = 2).

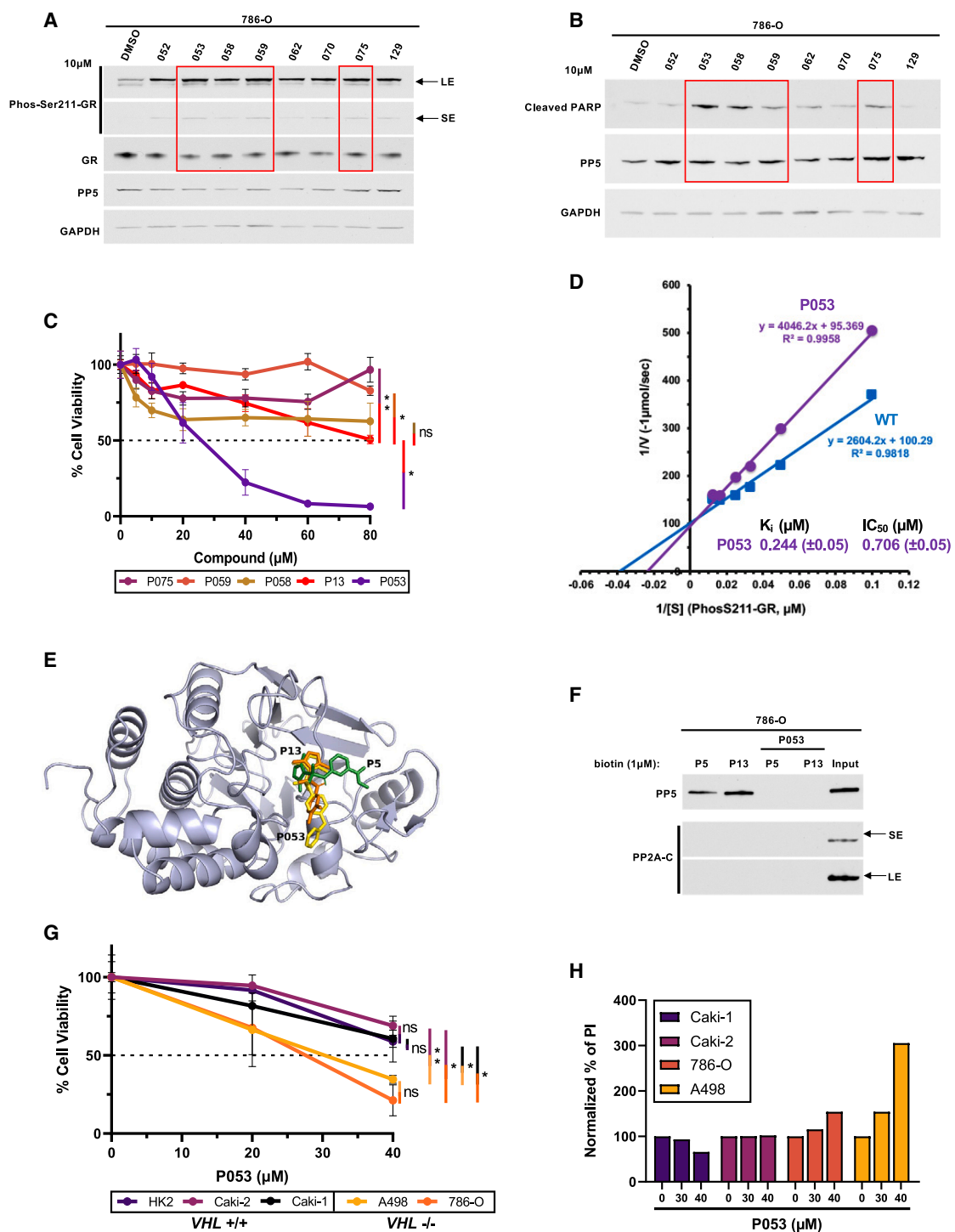


Figure 2. Inhibitory effect of P053 compound on PP5 and induction apoptosis in VHL-null ccRCC

(A) 786-O cells were treated with 10 μ M of the indicated second generation of PP5 inhibitors for 24 h. DMSO was used as control. PP5 inhibition was evaluated by immunoblotting for the *bona fide* substrate phospho-S211-GR. SE (short exposure) and LE (long exposure) of the radiographic film. GAPDH was used as a loading control.

(B) 786-O cells were treated with 10 μ M of the indicated second generation inhibitors of PP5 for 24 h. DMSO was used as control. Induction of apoptosis was evaluated by immunoblotting using apoptotic markers cleaved PARP and cleaved caspase-8. GAPDH was used as a loading control.

(C) 786-O cells were treated with indicated amounts of P13, P053, P058, P059, and P075 for 24 h and then cell proliferation was assessed by the MTT assay. A Student's *t* test was performed to assess statistical significance **p* < 0.05; ***p* < 0.01 or non-significant (ns).

(D) PP5 enzyme kinetic data with P053 (purple) or no inhibitor (blue line) presented as a Lineweaver–Burk plot (*n* = 3 independent samples).

(legend continued on next page)

with different amounts of biotin-P5 and biotin-P13 (Figure 1E). Our data suggest that PP5-FLAG binds to biotinylated P5 and P13. Furthermore, at 10 μ M biotin-P13 bound more to PP5-FLAG compared to biotin-P5 (Figure 1E). Due to the improved binding and activity of P13 relative to P5 we chose to continue further characterization with only P13.

We then mutated docking site residues in the active site of PP5 to obtain further insight into the mechanism of P13 binding to PP5. These included H304Q (catalytically inactive), M309C (prevents dephosphorylation of substrate phospho-Ser13-Cdc37), and W386F (hyperactivity against substrates) as well as additional mutants that help coordinate substrate binding based on our previously published work: R275A, R400A, and Y451F (Figure 1F).⁶ These mutants were transiently expressed in HEK293 cells, and then the protein lysates were challenged with different amounts of biotin-P13 (Figure 1G). Our data showed that H304Q, M309C, and W386F mutants were unable to bind to biotin-P13, confirming the P13 binding sites within the PP5 protein (Figure 1G). Additionally, the R400A mutant had reduced binding to biotin-P13 compared to the wild-type (WT) PP5 while R275A and Y451F had increased binding (Figure 1G).

We next synthesized BODIPY-labeled version of compound P13 (P13-BODIPY) in order to obtain the binding affinity of this inhibitor to PP5 *in vitro* (Figure S3A). This was accomplished by coupling the azidopropyl-P13 **10** with 4,4-difluoro-5,7-dimethyl-4-bora-3a,4a-diaza-s-indacene-3-propionic acid (BODIPY Acid **13**). Using fluorescence anisotropy with recombinant PP5 protein (Figure S3B), we determined the binding affinity of P13 compound to PP5 to be 376.2 ± 60 nM (Figure 1H).

Design, synthesis, and characterization of a more potent PP5 inhibitor

We next used an *in silico* docking strategy to design series of small molecule inhibitors of PP5 based on the structure of P13 as a starting point. Examination of the docking pose of compound P13 in the active site of PP5 where the isoxazole is coordinating to the metal ions yielded some ideas about modifications that could be beneficial for binding. Neighboring the binding site was a nonpolar pocket near W386 and M309, which might accommodate a tethered nonpolar group off the xylene ring of P13. Additionally, a more polar pocket near R400 and D388 might also be accessible for an alcohol or amide tethered through the sulfonamide nitrogen of P13. Using this model as a guide, a number of sulfonamide analogs were designed and docked into the PP5 active site using Autodock Vina. This docking gave a number of potential new PP5 inhibitors that were predicted to bind to the active site of PP5 with greater affinity than the parent P13 compound. This led to synthesis of a series of compounds: P052 (**16**), P053 (**20**), P058 (**22**), P059 (**17**), P062 (**18**), P070 (**19**), P075 (**23**), and P129 (**21**) (Figure S3C). Compounds **16** and **20** were syn-

thesized from the addition of the respective aniline to the isoxazole sulfonyl chloride **15** (Figures S3D–S3F). Further modification of the system was accomplished by alkylation with 3-chloropropyl *p*-toluenesulfonate to provide the alkyl chloride **17**. The chloride **17** could then be displaced with sodium azide to access azide **18**, which was then reduced to the amide and acylated to provide acetamide **19**. Alcohol **21** and sulfonamide **22** were prepared by alkylation of sulfonamide **16** with the appropriate alkyl halide, while nitrile **23** was prepared by displacement of alkyl chloride **17** with sodium cyanide.

We next treated the ccRCC cell line 786-O with 10 μ M of the compounds shown in Figure S3C for 18 h and confirmed that they inhibit PP5 as evidenced by increased phosphorylation of S211-GR, which is a known substrate of PP5 (Figure 2A). We next showed that only compounds P053, P058, P059, and P075 had the ability to induce apoptosis in 786-O cells (Figure 2B). We then treated 786-O cells with different amounts of P053, P058, P059, P075 as well as the parent compound P13 for 18 h and measured proliferation by MTT assay (Figure 2C). Compound P053 significantly inhibited the proliferation of 786-O cells compared to the other compounds including P13 (Figure 2C). Using our *in vitro* PP5 phosphatase specific assay we showed that P053 also is a competitive inhibitor of PP5 with K_i of 244 ± 50 nM (Figures 2D and S4A). Predicted P053 binding compared to P5 and P13 within PP5 protein structure is also demonstrated (Figure 2E). We next challenged the protein lysate from 786-O cells with 1 μ M biotin-P5 and P13 followed by competition with 1 μ M P053 compound (Figure 2F). Our data showed that 1 μ M P053 can compete and completely displace PP5 from biotin-P5 and P13 (Figure 2F). This suggests higher affinity of P053 toward PP5. It is also noteworthy that biotin-P5 and P13 did not bind to PP2A suggesting their specificity toward PP5 (Figure 2F). Our current, as well as previously published work,² has shown that PP5 plays a pro-survival role specifically in *VHL*-null ccRCC cells. We further demonstrated here that P053 significantly inhibited cell proliferation in *VHL*-null ccRCC cells, 786-O and A498 compared to normal epithelial renal cell HK2 as well as *VHL*-positive ccRCC cell lines Caki-1 and Caki-2 (Figures 2G and S4B). Using propidium iodide (PI) staining of the ccRCC cells treated with different amounts of P053 compound, we confirmed that P053 selectively caused cell death in *VHL*-null ccRCC cells in a dose-dependent manner (Figures 2H and S4C). Taken together, we have designed and synthesized a highly specific PP5 inhibitor that caused induction of apoptosis in *VHL*-null ccRCC.

PP5 attenuation induces extrinsic apoptosis in clear cell renal cell carcinoma

Our data obtained here as well as our previous work showed that pharmacologic inhibition or silencing of *PP5* in *VHL*-null ccRCC induced apoptosis.² Given this, we asked whether the observed

(E) The structure of PP5 catalytic domain (gray; PDB 3H60) bound to PP5 inhibitors P5 (green), P13 (orange), and P053 (yellow).

(F) Lysate from 786-O cells was collected and incubated with 1 μ M biotinylated P5 or P13 for 1 h and then challenged with 1 μ M P053 for 30 min. Streptavidin-coated agarose beads were used to pulldown the biotinylated compounds. Co-pulldown of endogenous PP5 and PP2A was assessed by immunoblotting. SE (short exposure) and LE (long exposure) of the radiographic film.

(G) *VHL* containing HK2, Caki-2, and Caki-1 cells and *VHL*-null cells, A498 and 786-O, were treated with the indicated amount of P053 for 24 h, and then cell proliferation was assessed by the MTT assay. A Student's *t* test was performed to assess statistical significance * $p < 0.05$; ** $p < 0.01$ or non-significant (ns).

(H) Caki-1, Caki-2, A498, and 786-O cells were treated with 30 or 40 μ M P053 or DMSO control (0 μ M) for 24 h. Following propidium iodide (PI) staining cell death was assessed by flow cytometry. Percentage of PI stained cells was normalized to the vehicle control for each cell line individually.

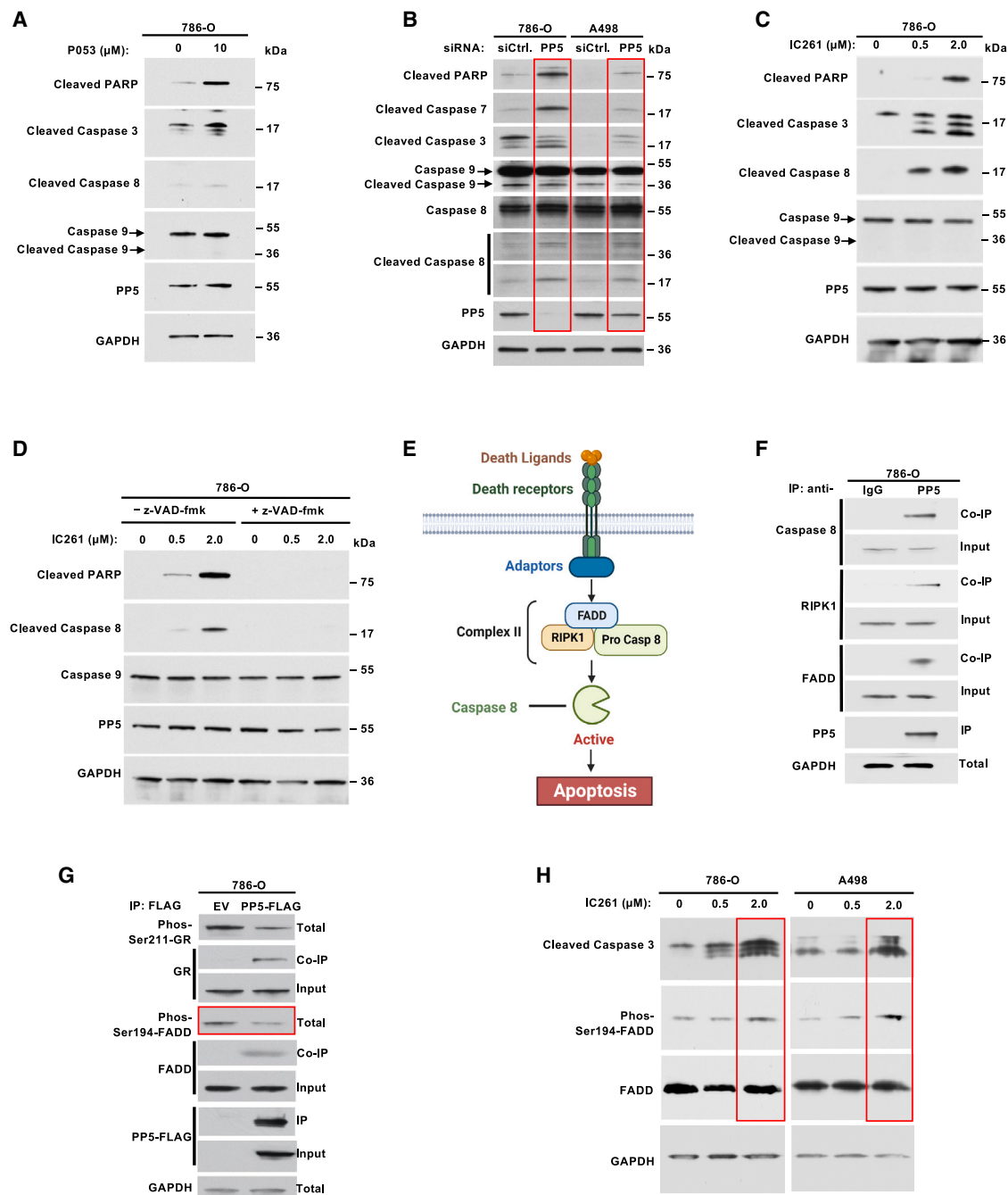


Figure 3. Targeting PP5 activates the extrinsic apoptotic pathway

(A) ccRCC 786-O cells were treated with 10 μM compound P053 for 24 h. Induction of apoptosis was evaluated by immunoblotting using apoptotic markers as indicated. GAPDH was used as a loading control.

(B) PP5 was silenced by small interfering RNA (siRNA) in VHL-null ccRCC cells 786-O and A498. Induction of apoptosis was evaluated by immunoblotting using apoptotic markers as indicated. siCtrl represents the non-targeting siRNA control. GAPDH was used as a loading control.

(C) Inhibition of CK1δ by indicated amounts of IC261 for 16 h in 786-O cells. Induction of apoptotic markers was assessed by immunoblotting. GAPDH was used as a loading control.

(D) ccRCC 786-O cells were treated in presence (+) or absence (-) of 10 μM apoptotic inhibitor z-VAD-fmk for 1 h followed by the addition of indicated amounts of CK1δ inhibitor, IC261, for an additional 16 h. Induction of apoptosis was evaluated by the immunoblotting. GAPDH was used as a loading control.

(E) Schematic representation of the extrinsic apoptotic pathway. Death receptors are activated by binding of death ligands. This leads to binding of adaptors and ultimately formation of complex II containing FADD, RIPK1, and pro-caspase-8. Upon complex II formation, caspase-8 is activated and then released from the complex leading to downstream caspase induction and apoptosis.

(F) Endogenous PP5 was immunoprecipitated (IP) from 786-O cells. Co-immunoprecipitation (co-IP) of FADD, RIPK1, and caspase-8 was examined by immunoblot. IgG was used as a control. GAPDH was used as a loading control.

(legend continued on next page)

apoptosis resulted from the intrinsic or extrinsic signaling pathway. First, treatment of *VHL*-null ccRCC lines 786-O with P053 caused increased cleavage of the executioner caspase-3 and the downstream target poly-ADP ribose polymerase (PARP), hallmarks of generalized cell death (Figure 3A). Interestingly, cleavage of caspase 8 but not caspase 9 indicated that PP5 inhibition resulted in activation of extrinsic apoptosis (Figure 3A). We obtained similar results with small interfering RNA (siRNA)-mediated knock-down (KD) of *PP5* in the *VHL*-null ccRCC lines 786-O and A498 (Figure 3B). T362-PP5 phosphorylation by CK1 δ is coupled to its activity.² We have shown that inhibition of CK1 δ using the small molecule IC261 decreased PP5 activity and induced apoptosis in *VHL*-null ccRCC cell lines.² Accordingly, treatment of 786-O cells with IC261 induced extrinsic apoptosis in a dose-dependent manner (Figure 3C). Inhibition of caspase activity using the pan-caspase inhibitor z-VAD-fmk reversed this effect (Figure 3D). Our data here suggests that KD or inhibition of PP5 activates the extrinsic apoptotic pathway in *VHL*-null ccRCC.

PP5 dephosphorylates FADD

To determine which aspect of extrinsic apoptosis is regulated by PP5, we examined PP5 association with extrinsic apoptosis proteins Fas-Associated by death domain (FADD) and receptor interacting serine/threonine kinase 1 (RIPK1). These two proteins, along with caspase-8, comprise complex II of the extrinsic apoptotic pathway (Figure 3E).^{31–34} We found that PP5 interacts with the members of complex II (Figure 3F). Immunoprecipitation (IP) of PP5 from 786-O cells demonstrated co-IP of FADD, RIPK1, and caspase-8 (Figure 3F).

Previous work has shown that phosphorylation of S194-FADD is important for its pro-apoptotic activity,³⁵ therefore, we hypothesized that PP5 targets and dephosphorylates S194-FADD to suppress apoptosis. Indeed, we found that overexpression of PP5 in 786-O cells led to decreased S194-FADD phosphorylation (Figure 3G). The *bona fide* PP5 substrate glucocorticoid receptor (S211-GR) has been included as a control for PP5 activity (Figure 3G). In further support of FADD as a PP5 substrate, siRNA-mediated KD of *PP5* in these cells led to increased phosphorylation of S194-FADD (Figure S4D). Additionally, we made a similar observation of increased phosphorylation of S194-FADD in CRISPR/Cas9 mediated-knockout (KO) of *PP5* in HAP1 cells (Figure S4E). In agreement with these findings, inhibition of PP5 activity in 786-O and A498 cells using IC261 led to an increase in S194-FADD phosphorylation (Figure 3H). Of note, overexpression of PP5-FLAG does not appear to impact the phosphorylation of S161-RIPK1 and S166-RIPK1 (Figure S4F). Taken together, our findings here indicate that PP5 can potentially regulate extrinsic apoptosis by dephosphorylating FADD.

PP5 associates with intact complex II

To gain further understanding of the dynamic of PP5 interaction with complex II, we used CRISPR/Cas9-mediated knockout (KO) of *PP5*, *FADD*, and *RIPK1* in HAP1 cells. These haploid cell lines

are a great resource for gene deletion in mammalian cells.³⁶ Immunoprecipitation (IP) of FADD from *PP5* KO cells showed FADD interaction with RIPK1 was abrogated (Figure 4A). Similarly, IP of RIPK1 from these cells also demonstrated loss of interaction with FADD (Figure 4A), therefore indicating that PP5 is necessary for mediating FADD:RIPK1 complex formation. We then confirmed this model in both *FADD* and *RIPK1* KO HAP1 cells. Our data demonstrated interaction of PP5 and FADD was unaffected in *RIPK1* KO cells (Figure 4B). Likewise, interaction of PP5 and RIPK1 was maintained in *FADD* KO HAP1 cells (Figure 4C).

Previous work showed that FADD and RIPK1 interaction is dependent on their death domains.^{37,38} In order to determine whether the death domain (DD) is involved in complex formation with PP5 in a cellular context, we created truncated FADD (FADD- Δ DD) (Figure 4D) and RIPK1 (RIPK1- Δ DD)^{37–39} (Figure 4E) constructs that lack this death domain. PP5 failed only to co-IP with death domain-deleted FADD (FADD- Δ DD) (Figure 4D), demonstrating the requirement of this interaction domain for complex II assembly with PP5.

Since a vast majority of PP5 substrates are also clients of the molecular chaperone Hsp90, we asked whether RIPK1 and FADD are clients of this chaperone. We therefore performed a time course assay using the Hsp90 inhibitor SNX-2112 (2 μ M) in HEK293 cells. Upon inhibition of Hsp90 clients such as Tsc2, Akt and phos-Ser473-Akt were destabilized and degraded (Figure 4F).^{40,41} Consistent with previously published work,⁴² we observed decreased RIPK1 protein levels after 16 h treatment with SNX-2112 (Figure 4F). Notably, we did not observe a decrease in FADD levels throughout the time course (Figure 4F). These data suggest that RIPK1, but not FADD, is an Hsp90 client. To further understand the relationship between FADD and Hsp90, we immunoprecipitated endogenous FADD from 786-O cells and examined the co-IP of Hsp90 (Figure 4G). Consistent with our previous results, we saw FADD interaction with PP5, however, we did not observe any interaction between FADD and Hsp90 (Figure 4G). These data suggest that FADD and PP5 interact independently of Hsp90. Taken together, our data demonstrates PP5 functions to maintain complex II integrity by interacting with FADD and RIPK1 (Figure 4H).

DISCUSSION

PP5 plays a significant role in proliferation and survival of multiple cancers including kidney cancer.^{3,43} Our previous work has shown that downregulation of PP5 or pharmacologic inhibition of its regulator CK1 δ caused induction of apoptosis.² Here we dissected the induction of this pathway and demonstrated the direct involvement of PP5 in the extrinsic apoptotic pathway. Presence of functional PP5 appears to be important for interaction of FADD and RIPK1. Phosphorylation of S194-FADD has been shown previously to be important for its pro-apoptotic activity and suppresses tumorigenesis.^{35,44} Our

(G) WT-PP5-FLAG was transiently expressed and isolated from 786-O cells. Co-IP of FADD and GR was examined by immunoblotting. Phosphorylation level of S194-FADD was assessed by immunoblot. PP5 activity was evaluated by immunoblotting for the *bona fide* substrate phospho-S211-GR as a control. GAPDH was used as a loading control.

(H) CK1 δ was inhibited with indicated amounts of IC261 for 24 h in ccRCC cells 786-O and A498. Induction of apoptotic markers shown by immunoblotting using anti-cleaved caspase-3 antibody. Phosphorylation of S194-FADD was evaluated by western blot. GAPDH was used as a loading control.

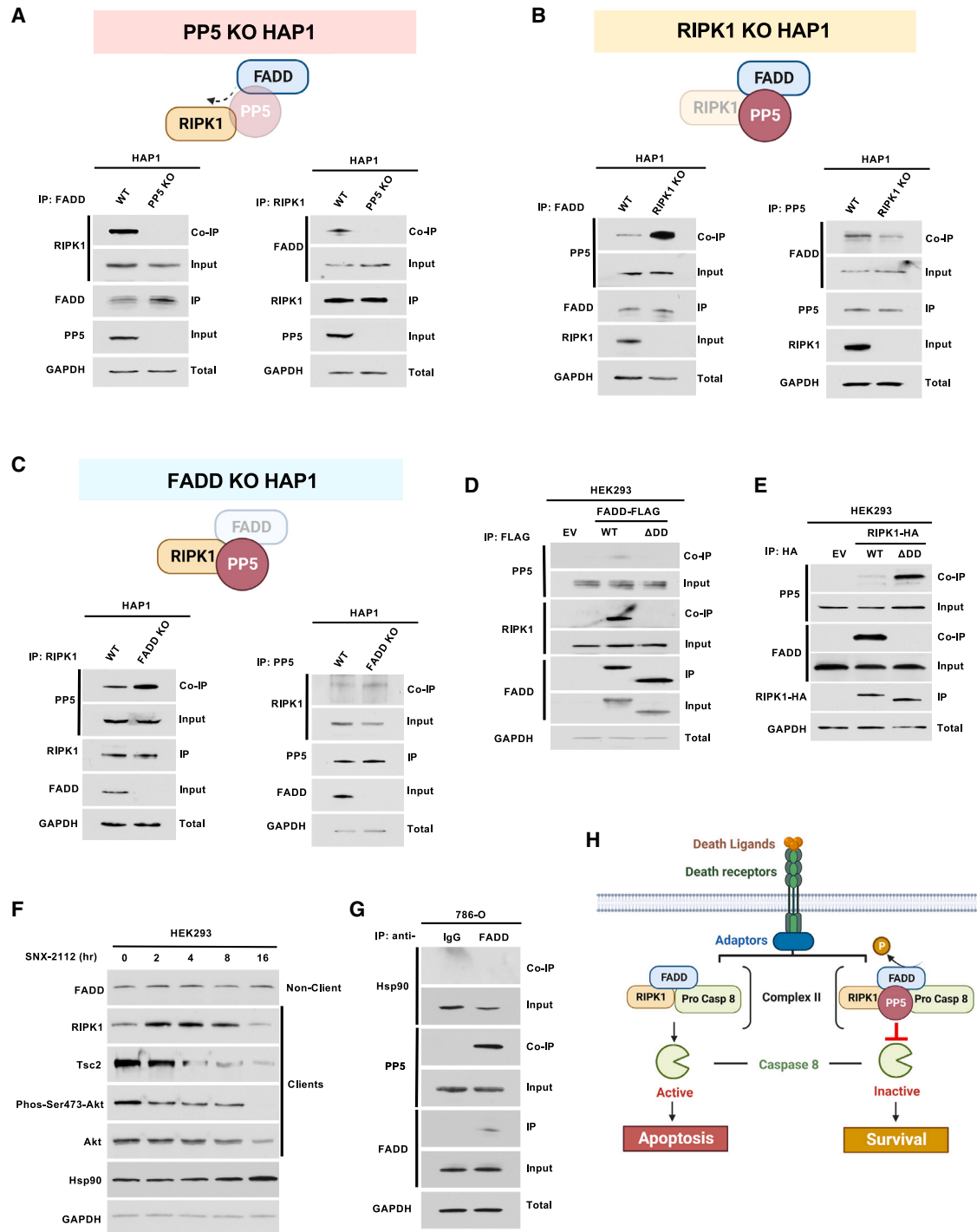


Figure 4. PP5 mediates complex II formation

(A) Endogenous FADD (left) and RIPK1 (right) were IP from WT-HAP1 and *PP5*-KO HAP1 cells. Co-IPs of RIPK1 and FADD were examined by immunoblot. GAPDH was used as a loading control.

(B) Endogenous FADD (left) and PP5 (right) were IP from WT-HAP1 and *RIPK1*-KO HAP1 cells. Co-IPs of PP5 and FADD were examined by immunoblot. GAPDH was used as a loading control.

(C) Endogenous RIPK1 (left) and PP5 (right) were IP from WT-HAP1 and *FADD*-KO HAP1 cells. Co-IPs of PP5 and RIPK1 were examined by immunoblot. GAPDH was used as a loading control.

(D) FADD-FLAG and death domain deleted FADD (FADD-FLAG- Δ DD) were transiently transfected and IP from HEK293 cells. EV was used as a control. Co-IP of RIPK1 and PP5 was examined by immunoblot. GAPDH was used as a loading control.

(legend continued on next page)

data suggest that PP5 mediates dephosphorylation of S194-FADD, independent of Hsp90 and facilitates FADD binding to RIPK1 via their death domains. The presence of active PP5 in complex II appears to maintain suppression of extrinsic apoptosis in *VHL*-null ccRCC and blocks the cleavage of caspase-8. Downregulation or inhibition of PP5 leads to increased phosphorylation of S194-FADD as well as cleavage of caspase-8 and induction of the extrinsic apoptotic pathway in *VHL*-null ccRCC. Of note, it has also been shown that many ccRCCs exhibit lower levels of FADD than adjacent normal kidney, however, it is not yet clear whether this may be related to PP5 upregulation and how FADD is functioning in that context.⁴⁵ Furthermore, S194-FADD phosphorylation has also been shown to regulate FADD function in cell cycle regulation.^{31,46,47} PP5 plays a number of roles in cell cycle regulation and this may be in part through FADD.

There are currently no reports of compounds that specifically inhibit PP5 function within cells.^{48–50} Zhang et al. designed a bifunctional molecule phosphatase recruiting chimera (PHORC) to specifically activate PP5 phosphatase activity toward the substrate Ask1.⁵¹ As PP5 is upregulated in a wide variety of cancers, a similar approach such as using proteolysis targeting chimeras (PROTACs) to specifically degrade PP5 may be beneficial for cancer therapy. Interestingly, LB-100, which has been developed as a specific PP2A inhibitor and is now in both phase 1 and phase 2 clinical trials for various cancers, has also been shown to inhibit PP5 and PP1.^{52–54} There are numerous reports highlighting the role of PP5 in cancer progression and survival due to its functions in cell cycle regulation, DNA damage response, and signaling pathways.³ These observations suggest a therapeutic benefit of PP5 inhibitors for the clinical treatment of wide variety cancers. Furthermore, the detailed molecular mechanism of the prosurvival role of PP5 in renal cancer prompted us to screen for and identify a small molecule inhibitor for this phosphatase. We took advantage of available X-ray crystal structures of the PP5 active site and performed 3-fold docking due to the promiscuity of PP5 to the metal ion in the active site, which can be a Zn, Mn, or an Fe ion. We chose residues D271, N303, H304, M309, and W386 to define the “active site” for docking, as these residues are near the metal ions in the active site of PP5.⁵ Our *in silico* screen and further cell-based assays led us to the identification of two compounds, P5 and P13. We further developed and synthesized the P053 compound based on P13. These inhibitors have high affinity (nM range) toward PP5 and appear to make contact with the active-site residues H304, M309, W386, and R400 within the substrate-binding pocket. We also found these compounds can bind to PP5 from *VHL*-null ccRCC and cause apoptosis in these cells. Interestingly, although the PP5 active-site residues are conserved in

other phosphatases such as PP2A, we did not observe any binding of our compounds to PP2AC, which is the catalytic subunit of PP2A, from cell lysate at the concentration at which they bound PP5.

The role of PP5 in cancer cell proliferation and survival as well as its unique structure make it an attractive therapeutic target. Important next steps for further evaluation of these PP5 inhibitors are to examine their pharmacokinetic and pharmacodynamic parameters as well as their effect on *VHL*-null ccRCC xenograft models. Examination in other cancers in which PP5 has been seen to play a pro-tumorigenic role is also warranted. Further refinement may be needed to optimize their on-target effects, but ultimately this work reveals a potential for small molecule PP5 inhibition in the clinic.

Limitations of the study

The PP5 inhibitors designed in this study bind specifically to and inhibit PP5 *in vitro* at nM range. However, in the cellular context, we used these PP5 inhibitors at low μ M in order to achieve apoptosis in ccRCC cell lines. Although we do not currently have experimental evidence, there are a number of reasons that can potentially explain this phenomenon. For instance, these drugs must cross the plasma membrane to enter the cell and inhibit the target, and therefore higher amounts are needed to achieve a potent inhibitory effect. Additionally, the PP5 protein used in our biochemical analysis was expressed and purified from bacteria, and therefore it is devoid of any posttranslational modifications. However, PP5 targeted in ccRCC cells is subjected to various posttranslational modifications² and this may potentially impact the binding affinity to the small molecule inhibitors of PP5.

SIGNIFICANCE

Protein phosphatase 5 is a serine/threonine phosphatase and a co-chaperone of Hsp90 that helps regulate an array of cellular functions including stress response, proliferation, apoptosis, and DNA repair.³ PP5 plays a significant role in survival and propagation of multiple cancers, which makes it a promising target for cancer therapy. Though there are several naturally occurring phosphatase inhibitors, none are specific for PP5. Additionally, the detailed molecular mechanism of PP5 prosurvival role in cancer has remained elusive. In this manuscript we have addressed these two overarching gaps in our knowledge. We previously solved the X-ray crystal structure of PP5 bound to its substrate peptide Cdc37.⁵ We used this information as well as other X-ray crystal structures of PP5 to conduct an *in silico* drug screen. This led to identification and development of selective and

(E) RIPK1-HA and death domain deleted RIPK1 (RIPK1-HA- Δ DD) were transiently transfected and isolated from HEK293 cells. EV was used as a control. Co-IP of FADD and PP5 was examined by immunoblot. GAPDH was used as a loading control.

(F) HEK293 cells were treated with 2 μ M SNX-2112 for the indicated times. FADD and RIPK1 protein levels were examined by immunoblot. *Bona fide* Hsp90 clients Tsc2, Akt and phos-Ser473-Akt were used as a positive control. GAPDH was used as a loading control.

(G) FADD was IP from 786-O cells. Co-IP of PP5 and Hsp90 was evaluated by immunoblot. IgG was used as a negative control. GAPDH was used as a loading control.

(H) Schematic illustration of PP5-mediated downregulation of the extrinsic apoptotic pathway. On the left, in the absence of PP5, following activation of the death receptors and complex II formation, caspase-8 is cleaved resulting in activation of apoptosis. On the right, when PP5 associates with complex II and dephosphorylates FADD on S194, the downstream apoptotic pathway is suppressed and leads to ccRCC cell survival.

competitive inhibitors of PP5. To our knowledge, this is the first known compound that specifically targets only the PP5 phosphatase. The second part of this story focuses on dissecting the molecular mechanism of PP5 in cancer cell survival. We previously reported the prosurvival role of PP5 in kidney cancer.² In this study we provide a mechanistic understanding of PP5 role in cells. We demonstrated that PP5 interacts with FADD, RIPK1, and caspase-8, components of the extrinsic apoptotic pathway complex II. Specifically, PP5 dephosphorylates and inactivates the death effector protein FADD in an Hsp90 independent manner, therefore preserving complex II integrity and regulating extrinsic apoptosis. Small molecule inhibition of PP5 activates this pathway, presenting a viable therapeutic strategy for renal cancer.

STAR★METHODS

Detailed methods are provided in the online version of this paper and include the following:

- KEY RESOURCES TABLE
- RESOURCE AVAILABILITY
 - Lead contact
 - Materials availability
 - Data and code availability
- EXPERIMENTAL MODEL AND STUDY PARTICIPANT DETAILS
 - Cell lines
 - Plasmids
- METHOD DETAILS
 - Cell transfection and treatment
 - Protein extraction, immunoprecipitation, and immunoblotting
 - Bacterial expression and protein purification of PP5
 - Cell viability assay
 - In silico docking
 - Synthesis of small molecules
 - Binding measurements and anisotropy
 - PP5 phosphatase activity and inhibition assay
 - Flow cytometric analysis
 - Biotin-P5 and biotin-P13 pulldown
- QUANTIFICATION AND STATISTICAL ANALYSIS

SUPPLEMENTAL INFORMATION

Supplemental information can be found online at <https://doi.org/10.1016/j.chembiol.2023.06.026>.

ACKNOWLEDGMENTS

We are grateful to Dr Laurence Pearl (University of Sussex) for his constructive comments. This work was supported by the National Institute of General Medical Sciences of the National Institutes of Health (NIH) under Award Number R01GM139932 (D.B.), R35GM139584 (M.M.) and Department of Defense (DOD) Kidney Cancer Research Program (KCRP) grant number KC190038 (J.D.C., M.M.). The content is solely the responsibility of the authors and does not necessarily represent the official views of the NIH or DoD. This work was also supported with funds from the SUNY Upstate Medical University, Upstate Foundation and Upstate Cancer Center (M.M.). Schematics in Figures 3 and 4 were created with [BioRender.com](https://www.biorender.com).

AUTHOR CONTRIBUTIONS

Conceptualization of the project G.B., D.B., J.D.C., I.N., and M.M.; experimental design, investigation, data analysis, and presentation, E.F.A., R.A.S., S.J.B., D.M.D., N.D., A.R.B., N.A.M., T.S., T.A., M.R., J.O., C.P., M.D., G.B., M.R.W., J.D.C., M.M.; original draft, E.A., R.A.S., S.J.B., M.R.W., M.M.; contributions to manuscript writing, review, and editing E.A., R.A.S., J.D.C., D.B., M.M.; and supervision, J.D.C. and M.M. All authors read the manuscript and provided their final approval for the content.

DECLARATION OF INTERESTS

The authors declare no competing financial interests.

INCLUSION AND DIVERSITY

We support inclusive, diverse, and equitable conduct of research.

Received: March 8, 2023

Revised: May 11, 2023

Accepted: June 30, 2023

Published: July 31, 2023

REFERENCES

1. Golden, T., Aragon, I.V., Rutland, B., Tucker, J.A., Shevde, L.A., Samant, R.S., Zhou, G., Amable, L., Skarra, D., and Honkanen, R.E. (2008). Elevated levels of Ser/Thr protein phosphatase 5 (PP5) in human breast cancer. *Biochim. Biophys. Acta* 1782, 259–270. <https://doi.org/10.1016/j.bbadis.2008.01.004>.
2. Dushukyan, N., Dunn, D.M., Sager, R.A., Woodford, M.R., Loisel, D.R., Daneshvar, M., Baker-Williams, A.J., Chisholm, J.D., Truman, A.W., Vaughan, C.K., et al. (2017). Phosphorylation and Ubiquitination Regulate Protein Phosphatase 5 Activity and Its Prosurvival Role in Kidney Cancer. *Cell Rep.* 21, 1883–1895. <https://doi.org/10.1016/j.celrep.2017.10.074>.
3. Sager, R.A., Dushukyan, N., Woodford, M., and Mollapour, M. (2020). Structure and function of the co-chaperone protein phosphatase 5 in cancer. *Cell Stress Chaperones* 25, 383–394. <https://doi.org/10.1007/s12192-020-01091-3>.
4. Oberoi, J., Guiu, X.A., Outwin, E.A., Schellenberger, P., Roumeliotis, T.I., Choudhary, J.S., and Pearl, L.H. (2022). HSP90-CDC37-PP5 forms a structural platform for kinase dephosphorylation. *Nat. Commun.* 13, 7343. <https://doi.org/10.1038/s41467-022-35143-2>.
5. Jaime-Garza, M., Nowotny, C.A., Coutandin, D., Wang, F., Tabios, M., and Agard, D.A. (2023). Hsp90 provides a platform for kinase dephosphorylation by PP5. *Nat. Commun.* 14, 2197. <https://doi.org/10.1038/s41467-023-37659-7>.
6. Oberoi, J., Dunn, D.M., Woodford, M.R., Mariotti, L., Schulman, J., Bourbouli, D., Mollapour, M., and Vaughan, C.K. (2016). Structural and functional basis of protein phosphatase 5 substrate specificity. *Proc. Natl. Acad. Sci. USA* 113, 9009–9014. <https://doi.org/10.1073/pnas.1603059113>.
7. Shi, Y. (2009). Serine/threonine phosphatases: mechanism through structure. *Cell* 139, 468–484. <https://doi.org/10.1016/j.cell.2009.10.006>.
8. Schopf, F.H., Biebl, M.M., and Buchner, J. (2017). The HSP90 chaperone machinery. *Nat. Rev. Mol. Cell Biol.* 18, 345–360. <https://doi.org/10.1038/nrm.2017.20>.
9. Cox, M.B., and Johnson, J.L. (2011). The Role of p23, Hop, Immunophilins, and Other Co-chaperones in Regulating Hsp90 Function. *Methods Mol. Biol.* 787, 45–66. https://doi.org/10.1007/978-1-61779-295-3_4.
10. Cliff, M.J., Harris, R., Barford, D., Ladbury, J.E., and Williams, M.A. (2006). Conformational diversity in the TPR domain-mediated interaction of protein phosphatase 5 with Hsp90. *Structure* 14, 415–426. <https://doi.org/10.1016/j.str.2005.12.009>.
11. Hasibeck, V., Eckl, J.M., Drazic, A., Rutz, D.A., Lorenz, O.R., Zimmermann, K., Kriehuber, T., Lindemann, C., Madl, T., and Richter, K.

- (2015). The activity of protein phosphatase 5 towards native clients is modulated by the middle- and C-terminal domains of Hsp90. *Sci. Rep.* 5, 17058. <https://doi.org/10.1038/srep17058>.
12. Kang, H., Sayner, S.L., Gross, K.L., Russell, L.C., and Chinkers, M. (2001). Identification of amino acids in the tetratricopeptide repeat and C-terminal domains of protein phosphatase 5 involved in autoinhibition and lipid activation. *Biochemistry* 40, 10485–10490.
13. Ramsey, A.J., and Chinkers, M. (2002). Identification of potential physiological activators of protein phosphatase 5. *Biochemistry* 41, 5625–5632.
14. Yang, J., Roe, S.M., Cliff, M.J., Williams, M.A., Ladbury, J.E., Cohen, P.T.W., and Barford, D. (2005). Molecular basis for TPR domain-mediated regulation of protein phosphatase 5. *EMBO J.* 24, 1–10. <https://doi.org/10.1038/sj.emboj.7600496>.
15. Zeke, T., Morrice, N., Vázquez-Martin, C., and Cohen, P.T.W. (2005). Human protein phosphatase 5 dissociates from heat-shock proteins and is proteolytically activated in response to arachidonic acid and the microtubule-depolymerizing drug nocodazole. *Biochem. J.* 385, 45–56. <https://doi.org/10.1042/BJ20040690> [BJ20040690](https://doi.org/10.1042/BJ20040690) [pii].
16. Vaughan, C.K., Mollapour, M., Smith, J.R., Truman, A., Hu, B., Good, V.M., Panaretou, B., Neckers, L., Clarke, P.A., Workman, P., et al. (2008). Hsp90-dependent activation of protein kinases is regulated by chaperone-targeted dephosphorylation of Cdc37. *Mol. Cell.* 31, 886–895. <https://doi.org/10.1016/j.molcel.2008.07.021>.
17. Chatterjee, A., Wang, L., Armstrong, D.L., and Rossie, S. (2010). Activated Rac1 GTPase translocates protein phosphatase 5 to the cell membrane and stimulates phosphatase activity in vitro. *J. Biol. Chem.* 285, 3872–3882. <https://doi.org/10.1074/jbc.M109.088427>.
18. Clifford, S.C., Astuti, D., Hooper, L., Maxwell, P.H., Ratcliffe, P.J., and Maher, E.R. (2001). The pVHL-associated SCF ubiquitin ligase complex: molecular genetic analysis of elongin B and C, Rbx1 and HIF-1alpha in renal cell carcinoma. *Oncogene* 20, 5067–5074. <https://doi.org/10.1038/sj.onc.1204602>.
19. Maxwell, P.H., Wiesener, M.S., Chang, G.W., Clifford, S.C., Vaux, E.C., Cockman, M.E., Wykoff, C.C., Pugh, C.W., Maher, E.R., and Ratcliffe, P.J. (1999). The tumour suppressor protein VHL targets hypoxia-inducible factors for oxygen-dependent proteolysis. *Nature* 399, 271–275. <https://doi.org/10.1038/20459>.
20. Kondo, K., Klco, J., Nakamura, E., Lechpammer, M., and Kaelin, W.G., Jr. (2002). Inhibition of HIF is necessary for tumor suppression by the von Hippel-Lindau protein. *Cancer Cell* 1, 237–246.
21. Woodford, M.R., Backe, S.J., Wengert, L.A., Dunn, D.M., Bourboulia, D., and Mollapour, M. (2021). Hsp90 chaperone code and the tumor suppressor VHL cooperatively regulate the mitotic checkpoint. *Cell Stress Chaperones* 26, 965–971. <https://doi.org/10.1007/s12192-021-01240-2>.
22. Hasanov, E., Chen, G., Chowdhury, P., Weldon, J., Ding, Z., Jonasch, E., Sen, S., Walker, C.L., and Dere, R. (2017). Ubiquitination and regulation of AURKA identifies a hypoxia-independent E3 ligase activity of VHL. *Oncogene* 36, 3450–3463. <https://doi.org/10.1038/onc.2016.495>.
23. Bluysen, H.A.R., Lolkema, M.P.J.K., van Beest, M., Boone, M., Sniijckers, C.M.J.T., Los, M., Gebbink, M.F.B.G., Braam, B., Holstege, F.C.P., Giles, R.H., and Voest, E.E. (2004). Fibronectin is a hypoxia-independent target of the tumor suppressor VHL. *FEBS Lett.* 556, 137–142. [https://doi.org/10.1016/s0014-5793\(03\)01392-9](https://doi.org/10.1016/s0014-5793(03)01392-9).
24. Linehan, W.M., Schmidt, L.S., Crooks, D.R., Wei, D., Srinivasan, R., Lang, M., and Ricketts, C.J. (2019). The Metabolic Basis of Kidney Cancer. *Cancer Discov.* 9, 1006–1021. <https://doi.org/10.1158/2159-8290.CD-18-1354>.
25. Choueiri, T.K., and Kaelin, W.G., Jr. (2020). Targeting the HIF2-VEGF axis in renal cell carcinoma. *Nat. Med.* 26, 1519–1530. <https://doi.org/10.1038/s41591-020-1093-z>.
26. Iliopoulos, O., Kibel, A., Gray, S., and Kaelin, W.G., Jr. (1995). Tumour suppression by the human von Hippel-Lindau gene product. *Nat. Med.* 1, 822–826.
27. Bertini, I., Calderone, V., Fragai, M., Luchinat, C., and Talluri, E. (2009). Structural basis of serine/threonine phosphatase inhibition by the archetypal small molecules cantharidin and norcantharidin. *J. Med. Chem.* 52, 4838–4843. <https://doi.org/10.1021/jm900610k>.
28. Irwin, J.J. (2008). Using ZINC to acquire a virtual screening library. *Curr. Protoc. Bioinformatics Chapter 14*, 14.6.1–14.6.23. Unit 14 16. <https://doi.org/10.1002/0471250953.bi1406s22>.
29. Irwin, J.J., Raushel, F.M., and Shoichet, B.K. (2005). Virtual screening against metalloenzymes for inhibitors and substrates. *Biochemistry* 44, 12316–12328. <https://doi.org/10.1021/bi050801k>.
30. Irwin, J.J., Shoichet, B.K., Mysinger, M.M., Huang, N., Colizzi, F., Wassam, P., and Cao, Y. (2009). Automated docking screens: a feasibility study. *J. Med. Chem.* 52, 5712–5720. <https://doi.org/10.1021/jm9006966>.
31. Alappat, E.C., Feig, C., Boyerinas, B., Volkland, J., Samuels, M., Murrmann, A.E., Thorburn, A., Kidd, V.J., Slaughter, C.A., Osborn, S.L., et al. (2005). Phosphorylation of FADD at serine 194 by CK1alpha regulates its nonapoptotic activities. *Mol. Cell.* 19, 321–332. <https://doi.org/10.1016/j.molcel.2005.06.024>.
32. Lee, E.W., Kim, J.H., Ahn, Y.H., Seo, J., Ko, A., Jeong, M., Kim, S.J., Ro, J.Y., Park, K.M., Lee, H.W., et al. (2012). Ubiquitination and degradation of the FADD adaptor protein regulate death receptor-mediated apoptosis and necroptosis. *Nat. Commun.* 3, 978. <https://doi.org/10.1038/ncomms1981>.
33. Lee, E.W., Seo, J., Jeong, M., Lee, S., and Song, J. (2012). The roles of FADD in extrinsic apoptosis and necroptosis. *BMB Rep.* 45, 496–508. <https://doi.org/10.5483/bmbrep.2012.45.9.186>.
34. Lee, H.J., Pyo, J.O., Oh, Y., Kim, H.J., Hong, S.H., Jeon, Y.J., Kim, H., Cho, D.H., Woo, H.N., Song, S., et al. (2007). AK2 activates a novel apoptotic pathway through formation of a complex with FADD and caspase-10. *Nat. Cell Biol.* 9, 1303–1310. <https://doi.org/10.1038/ncb1650>.
35. Shimada, K., Matsuyoshi, S., Nakamura, M., Ishida, E., Kishi, M., and Konishi, N. (2004). Phosphorylation of FADD is critical for sensitivity to anti-cancer drug-induced apoptosis. *Carcinogenesis* 25, 1089–1097. <https://doi.org/10.1093/carcin/bgh130>.
36. Kotecki, M., Reddy, P.S., and Cochran, B.H. (1999). Isolation and characterization of a near-haploid human cell line. *Exp. Cell Res.* 252, 273–280. <https://doi.org/10.1006/excr.1999.4656>.
37. Meng, H., Liu, Z., Li, X., Wang, H., Jin, T., Wu, G., Shan, B., Christofferson, D.E., Qi, C., Yu, Q., et al. (2018). Death-domain dimerization-mediated activation of RIPK1 controls necroptosis and RIPK1-dependent apoptosis. *Proc. Natl. Acad. Sci. USA* 115, E2001–E2009. <https://doi.org/10.1073/pnas.1722013115>.
38. Vanden Berghe, T., van Loo, G., Saelens, X., Van Gurp, M., Brouckaert, G., Kalai, M., Declercq, W., and Vandenabeele, P. (2004). Differential signaling to apoptotic and necrotic cell death by Fas-associated death domain protein FADD. *J. Biol. Chem.* 279, 7925–7933. <https://doi.org/10.1074/jbc.M307807200> [M307807200](https://doi.org/10.1074/jbc.M307807200) [pii].
39. Seo, J., Lee, E.W., Sung, H., Seong, D., Dondelinger, Y., Shin, J., Jeong, M., Lee, H.K., Kim, J.H., Han, S.Y., et al. (2016). CHIP controls necroptosis through ubiquitylation- and lysosome-dependent degradation of RIPK3. *Nat. Cell Biol.* 18, 291–302. <https://doi.org/10.1038/ncb3314>.
40. Woodford, M.R., Sager, R.A., Marris, E., Dunn, D.M., Blanden, A.R., Murphy, R.L., Rensing, N., Shapiro, O., Panaretou, B., Prodromou, C., et al. (2017). Tumor suppressor Tsc1 is a new Hsp90 co-chaperone that facilitates folding of kinase and non-kinase clients. *EMBO J.* 36, 3650–3665. <https://doi.org/10.15252/emboj.201796700>.
41. Barrott, J.J., Hughes, P.F., Osada, T., Yang, X.Y., Hartman, Z.C., Loiselle, D.R., Spector, N.L., Neckers, L., Rajaram, N., Hu, F., et al. (2013). Optical and radioiodinated tethered Hsp90 inhibitors reveal selective internalization of ectopic Hsp90 in malignant breast tumor cells. *Chem. Biol.* 20, 1187–1197. <https://doi.org/10.1016/j.chembiol.2013.08.004>.
42. Yang, C.K., and He, S.D. (2016). Heat shock protein 90 regulates necroptosis by modulating multiple signaling effectors. *Cell Death Dis.* 7, e2126. <https://doi.org/10.1038/cddis.2016.25>.

43. D'Arcy, B.M., Prakash, A., and Honkanen, R.E. (2019). Targeting phosphatases in cancer: suppression of many versus the ablation of one. *Oncotarget* *10*, 6543–6545. <https://doi.org/10.18632/oncotarget.27201>.
44. Jang, M.S., Lee, S.J., Kim, C.J., Lee, C.W., and Kim, E. (2011). Phosphorylation by polo-like kinase 1 induces the tumor-suppressing activity of FADD. *Oncogene* *30*, 471–481. <https://doi.org/10.1038/onc.2010.423>.
45. Xu, H., He, L., Feng, X., Kapoor, A., and Tang, D. (2009). Specific reduction of fas-associated protein with death domain (FADD) in clear cell renal cell carcinoma. *Cancer Invest.* *27*, 836–843. <https://doi.org/10.1080/07357900902849681>.
46. Seyrek, K., Ivanisenko, N.V., Richter, M., Hillert, L.K., König, C., and Lavrik, I.N. (2020). Controlling Cell Death through Post-translational Modifications of DED Proteins. *Trends Cell Biol.* *30*, 354–369. <https://doi.org/10.1016/j.tcb.2020.02.006>.
47. Vilmont, V., Filhol, O., Hesse, A.M., Couté, Y., Hue, C., Rémy-Tourneur, L., Mistou, S., Cochet, C., and Chiochia, G. (2015). Modulatory role of the anti-apoptotic protein kinase CK2 in the sub-cellular localization of Fas associated death domain protein (FADD). *Biochim. Biophys. Acta* *1853*, 2885–2896. <https://doi.org/10.1016/j.bbamcr.2015.08.001>.
48. Swingle, M.R., and Honkanen, R.E. (2014). Development and validation of a robust and sensitive assay for the discovery of selective inhibitors for serine/threonine protein phosphatases PP1alpha (PPP1C) and PP5 (PPP5C). *Assay Drug Dev. Technol.* *12*, 481–496. <https://doi.org/10.1089/adt.2014.603>.
49. Liu, J.Y., Chen, X.E., and Zhang, Y.L. (2015). Insights into the key interactions between human protein phosphatase 5 and cantharidin using molecular dynamics and site-directed mutagenesis bioassays. *Sci. Rep.* *5*, 12359. <https://doi.org/10.1038/srep12359>.
50. Swingle, M., Volmar, C.H., Saldanha, S.A., Chase, P., Eberhart, C., Salter, E.A., D'Arcy, B., Schroeder, C.E., Golden, J.E., Wierzbicki, A., et al. (2017). An Ultra-High-Throughput Screen for Catalytic Inhibitors of Serine/Threonine Protein Phosphatases Types 1 and 5 (PP1C and PP5C). *SLAS Discov.* *22*, 21–31. <https://doi.org/10.1177/1087057116668852>.
51. Zhang, Q., Wu, X., Zhang, H., Wu, Q., Fu, M., Hua, L., Zhu, X., Guo, Y., Zhang, L., You, Q., and Wang, L. (2023). Protein Phosphatase 5-Recruiting Chimeras for Accelerating Apoptosis-Signal-Regulated Kinase 1 Dephosphorylation with Antiproliferative Activity. *J. Am. Chem. Soc.* *145*, 1118–1128. <https://doi.org/10.1021/jacs.2c10759>.
52. Hong, C.S., Ho, W., Zhang, C., Yang, C., Elder, J.B., and Zhuang, Z. (2015). LB100, a small molecule inhibitor of PP2A with potent chemo- and radio-sensitizing potential. *Cancer Biol. Ther.* *16*, 821–833. <https://doi.org/10.1080/15384047.2015.1040961>.
53. D'Arcy, B.M., Swingle, M.R., Papke, C.M., Abney, K.A., Bouska, E.S., Prakash, A., and Honkanen, R.E. (2019). The Antitumor Drug LB-100 Is a Catalytic Inhibitor of Protein Phosphatase 2A (PPP2CA) and 5 (PPP5C) Coordinating with the Active-Site Catalytic Metals in PPP5C. *Mol. Cancer Therapeut.* *18*, 556–566. <https://doi.org/10.1158/1535-7163.MCT-17-1143>.
54. Shuhaibar, L.C., Kaci, N., Egbert, J.R., Horville, T., Loisy, L., Vigone, G., Uliasz, T.F., Dambroise, E., Swingle, M.R., Honkanen, R.E., et al. (2021). Phosphatase inhibition by LB-100 enhances BMN-111 stimulation of bone growth. *JCI Insight* *6*, e141426. <https://doi.org/10.1172/jci.insight.141426>.
55. Mollapour, M., Tsutsumi, S., Donnelly, A.C., Beebe, K., Tokita, M.J., Lee, M.J., Lee, S., Morra, G., Bourboullia, D., Scroggins, B.T., et al. (2010). Swe1Wee1-dependent tyrosine phosphorylation of Hsp90 regulates distinct facets of chaperone function. *Mol. Cell.* *37*, 333–343. <https://doi.org/10.1016/j.molcel.2010.01.005>.
56. Woodford, M.R., Truman, A.W., Dunn, D.M., Jensen, S.M., Cotran, R., Bullard, R., Abouelleil, M., Beebe, K., Wolfgeher, D., Wierzbicki, S., et al. (2016). Mps1 Mediated Phosphorylation of Hsp90 Confers Renal Cell Carcinoma Sensitivity and Selectivity to Hsp90 Inhibitors. *Cell Rep.* *14*, 872–884. <https://doi.org/10.1016/j.celrep.2015.12.084>.
57. Trott, O., and Olson, A.J. (2010). AutoDock Vina: improving the speed and accuracy of docking with a new scoring function, efficient optimization, and multithreading. *J. Comput. Chem.* *31*, 455–461. <https://doi.org/10.1002/jcc.21334>.
58. Krajcovicova, S., Stankova, J., Dzubak, P., Hajduch, M., Soural, M., and Urban, M. (2018). A Synthetic Approach for the Rapid Preparation of BODIPY Conjugates and their use in Imaging of Cellular Drug Uptake and Distribution. *Chemistry* *24*, 4957–4966. <https://doi.org/10.1002/chem.201706093>.
59. White, J., and Whiteley, C.G. (1993). Use of Organoboranes in the Synthesis of Pheromones: A Convenient Synthesis of (Z)-6-Heneicosen-11-one and (Z)-5-Undecen-2-one, Pheromones from the Douglas Fir Tussock Moth and the Bontebok, Respectively. *Synthesis*, 1141–1144. <https://doi.org/10.1055/s-1993-26016>.
60. Cer, R.Z., Mudunuri, U., Stephens, R., and Lebeda, F.J. (2009). IC50-to-Ki: a web-based tool for converting IC50 to Ki values for inhibitors of enzyme activity and ligand binding. *Nucleic Acids Res.* *37*, W441–W445. <https://doi.org/10.1093/nar/gkp253>.

STAR★METHODS

KEY RESOURCES TABLE

REAGENT or RESOURCE	SOURCE	IDENTIFIER
Antibodies		
Rabbit anti-FLAG tag	Thermo Scientific	Cat# PA1-984B; RRID:AB_347227
Rabbit anti-HA tag (C29F4)	Cell Signaling Technology	Cat# 3724; RRID:AB_1549585
Mouse anti-6x-His epitope tag (HIS.H8)	Thermo Scientific	Cat# MA1-21315; RRID:AB_557403
Mouse anti-GAPDH (1D4)	Enzo Life Sciences	Cat# ADI-CSA-335; RRID:AB_10617247
Rabbit anti-PP5	Cell Signaling Technology	Cat# 2289; RRID:AB_2168757
Mouse anti-PP5 (2E12)	Abcam	Cat# ab123919; RRID:AB_10976136
Rabbit anti-FADD	Cell Signaling Technology	Cat# 2782; RRID:AB_2100484
Rabbit anti-phos-Ser194-FADD	Cell Signaling Technology	Cat# 2781; RRID:AB_2100485
Rabbit anti-RIPK1	Cell Signaling Technology	Cat# 3493; RRID:AB_2305314
Rabbit anti-phos-Ser161-RIPK1	Invitrogen	Cat# PA5-105640; RRID:AB_2817068
Rabbit anti-phos-Ser166-RIPK1	Cell Signaling Technology	Cat# 44590; RRID:AB_2799268
Rabbit anti-phos-Ser13-Cdc37 (EPR4979)	Abcam	Cat# ab108360; RRID:AB_10859480
Rabbit anti-Cdc37	StressMarq Biosciences	Cat# SPC-142; RRID:AB_2570605
Rabbit anti-GR (D6H2L)	Cell Signaling Technology	Cat# 12041; RRID:AB_2631286
Mouse anti-GR (D4X9S)	Cell Signaling Technology	Cat# 47411; RRID:AB_2799324
Rabbit anti-phospho-GR S211	Cell Signaling Technology	Cat# 4161; RRID:AB_2155797
Rabbit anti-cleaved-PARP	Cell Signaling Technology	Cat# 5625; RRID:AB_10699459
Rabbit anti-caspase-3	Cell Signaling Technology	Cat# 9665; RRID:AB_2069872
Rabbit anti-cleaved caspase-3	Cell Signaling Technology	Cat# 9664; RRID:AB_2070042
Rabbit anti-cleaved caspase-7	Cell Signaling Technology	Cat# 9491; RRID:AB_2068144
Mouse anti-caspase-9	Cell Signaling Technology	Cat# 9508; RRID:AB_2068620
Mouse anti-caspase-8	Cell Signaling Technology	Cat# 9746; RRID:AB_2275120
Rabbit anti-cleaved caspase-8	Cell Signaling Technology	Cat# 9496; RRID:AB_561381
Rabbit anti-PP2A C Subunit	Cell Signaling Technology	Cat# 2038; RRID:AB_2169495
Rabbit anti-VHL	Cell Signaling Technology	Cat# 68547; RRID:AB_2716279
Rabbit anti-phospho-Akt S473 (D9E)	Cell Signaling Technology	Cat# 2289; RRID:AB_2315049
Mouse anti-Akt (2H10)	Cell Signaling Technology	Cat# 2967; RRID:AB_331160
Rabbit Tuberin/TSC2 (D93F12) XP®	Cell Signaling Technology	Cat# 4308; RRID:AB_10547134
Rat anti-Hsp90 (16F1)	Enzo Life Sciences	Cat# ADI-SPA-835; RRID:AB_11181205
Anti-mouse secondary	Cell Signaling Technology	Cat# 7076; RRID:AB_330924
Anti-rabbit secondary	Cell Signaling Technology	Cat# 7074; RRID:AB_2099233
Bacterial and virus strains		
BL21(DE3)	EMD Millipore	Cat# 69450
DH5-alpha Electrocompetent E coli	Goldbio	Cat# CC-203
Chemicals, peptides, and recombinant proteins		
IC261	Abcam	Cat# ab145189
Z-VAD-FMK pan-caspase Inhibitor	Enzo Life Sciences	Cat# ALX-260-020-M001
PP5 (PPP5C) Human siRNA Oligo Duplex	OriGene Technologies	Cat# SR321403; SKU# SR321403A; SKU# SR321403B; SKU# SR321403C
Universal scrambled negative control siRNA duplex	OriGene Technologies	Cat# SR30004
Compound P0-P13	This Paper	N/A
Biotin-P5	This Paper	N/A
Biotin-P13	This Paper	N/A

(Continued on next page)

Continued

REAGENT or RESOURCE	SOURCE	IDENTIFIER
BODIPY-P13	This Paper	N/A
P13 derivatives	This Paper	N/A
Phos-Ser211-GR peptide ([NH ₂]PGKETNE[pS]PWRSDLL[COOH])	ThermoFisher Scientific custom synthesized	This paper
SNX2112	Duke University; Dr. Timothy Haystead ⁶¹	CAS# 908112-43-6

Critical Commercial Assays

Mirus TransIT-2020	MirusBio	Cat# MIR5405
Anti-FLAG M2 affinity gel	Sigma-Aldrich	Cat# A2220
Protein G agarose	ThermoFisher Scientific	Cat# 15-920-010
Pierce Anti-HA Agarose	ThermoFisher Scientific	Cat# PI26182
Ni-NTA Agarose	ThermoFisher Scientific	Cat# 88221
Quick Cell Proliferation Kit Plus	BioVision	Cat# K302-500; CAS# 150849-52-8
PIPer™ Phosphate Assay Kit	ThermoFisher Scientific	Cat# P22061
ANNEXIN V:FITC assay Kit	BIO-RAD	Cat# ANNEX300F

Experimental models: Cell lines

786-O	ATCC	Cat# CRL-1932
A498	ATCC	Cat# HTB-44
WT HAP-1	Horizon Discovery	Cat# C631
PP5 HAP-1 KO	Horizon Discovery	Cat# HZGHC003163c001
FADD HAP-1 KO	Horizon Discovery	Cat# HZGHC002596c006
RIPK1 HAP1-KO	Horizon Discovery	Cat# HZGHC000060c015
HEK293	ATCC	Cat# CRL-1573
HK-2	ATCC	Cat# CRL-2190
Caki-1	ATCC	Cat# HTB-46
Caki-2	ATCC	Cat# HTB-47

Oligonucleotides

DNA primers	Eurofins Genomics	See Table S1
-------------	-------------------	------------------------------

Recombinant DNA

pcDNA3-PP5-FLAG	Dushukyan et al. ²	N/A
pcDNA3-HA-RIPK1	Seo et al. ³⁹	Addgene plasmid # 78834; RRID:Addgene_78834
pcDNA3-FLAG-FADD	Lee et al. ³²	Addgene plasmid # 78802; RRID:Addgene_78802
pcDNA3-PP5-FLAG-M309C	Oberoi et al. ⁶	N/A
pcDNA3-PP5-FLAG-W386F	Oberoi et al. ⁶	N/A
pGEX6P1-PP5	Oberoi et al. ⁶	N/A

Software and algorithms

Biorender	Biorender, Toronto, ON M5V 2J1, Canada	https://biorender.com/
PyMOL version 2.5.4 for windows	Schrödinger, Inc. San Diego, CA, USA	https://pymol.org/2/
GraphPad Prism version 9.5.0 for windows	GraphPad Software, La Jolla, CA, USA,	www.graphpad.com
FlowJo 10.7.1 for windows	FlowJo, Ashland, OR, USA	https://www.flowjo.com/
Chemdraw 20.1	PerkinElmer, USA	https://perkinelmerinformatics.com/products/research/chemdraw

RESOURCE AVAILABILITY

Lead contact

Further information and requests for resources and reagents should be directed to and will be fulfilled by the lead contact, Mehdi Mollapour (mollapom@upstate.edu).

Materials availability

Plasmids generated in this study will be made available on request following a completed material transfer agreement.

Data and code availability

- The 200 compounds identified by the initial *in silico* screen reported in this paper will be shared by the [lead contact](#) upon request.
- This paper does not report original code.
- Any additional information required to reanalyze the data reported in this paper is available from the [lead contact](#) upon request.

EXPERIMENTAL MODEL AND STUDY PARTICIPANT DETAILS

Cell lines

Cultured human embryonic kidney (HEK293), (Human, unknown) and human kidney 2 (HK2), (Human, Male) cells were grown in Dulbecco's Modified Eagle Medium (DMEM, Sigma-Aldrich), 786-O cells (Human, Male) in Roswell Park Memorial Institute (RPMI) 1640 Medium (Sigma-Aldrich), A498 cells (Human, Female) in Minimum Essential Medium (MEM, Sigma-Aldrich), Caki-1 (Human, Male) and Caki-2 cells (Human, Male) in McCoy's 5A Medium (Sigma-Aldrich) and WT HAP1 (Human, Male) and knock-out (KO) cells (Human, Male) in Isocove's Modified Dulbecco's Medium (IMDM, Gibco), all supplemented with 10% fetal bovine serum (FBS, Sigma-Aldrich). WT-HAP1 and KO cell lines were acquired from Horizon Discovery. All other cell lines were obtained from (American Type Culture Collection, ATCC). Cells were maintained in a CellQ incubator (Panasonic Healthcare) at 37°C in an atmosphere containing 5% CO₂.

Plasmids

For mammalian expression, pcDNA3-PP5-FLAG and the M309C and W386F point mutations were created previously.^{2,6} Site-directed mutagenesis was performed to mutate R275A, H304Q, R400A, and Y451F residues (see [Table S1](#)) and confirmed by DNA sequencing. The pcDNA3-FLAG-FADD and pcDNA3-HA-RIPK1 were purchased from Addgene. FLAG-FADD-ΔDD as well as HA-RIPK1-ΔDD constructs were subcloned using the primers listed in [Table S1](#). For bacterial expression, we used our previously reported human *PP5* gene in pGEX6P1 plasmid with an N-terminal GST tag and C-terminal His₆ tag.⁶

METHOD DETAILS

Cell transfection and treatment

Cultured cells were split and then transfected the following day when about 40% confluent with each construct using Mirus TransIT-2020 (MirusBio) according to manufacturer's protocol. Cells were incubated at 37°C and then extracted or collected for analysis after 24hrs (HEK293) or 72hrs (ccRCC cell lines). Short interfering RNA (siRNA) scramble control and PPP5C (PP5) targeting duplexes were purchased from OriGene (SKU: SR321403A, SR321403B, and SR321403C). Indicated cells were transiently transfected with the siRNA using Mirus TransIT-2020. For PP5 knock-down, either 30 nM of control siRNA or 10 nM of each PP5 siRNA duplex (A, B and C) were mixed prior to transfection. Cells were incubated at 37°C for 72hrs, then harvested for protein extraction. To inhibit PP5 activity, 786-O cells were incubated with indicated amount of IC261 (Abcam) for 16hrs. Blockage of caspase activity was performed by treatment with 10 μM of z-VAD-fmk (Enzo Life Sciences) for 1 h followed by IC261 treatment with the indicated amount for 16hrs. Cells were then harvested for protein extraction.

Protein extraction, immunoprecipitation, and immunoblotting

Protein extraction from mammalian cells was carried out using methods previously described.^{55,56} Cell lysates were quantified using 1X Bradford reagent (Biorad). For immunoprecipitation, cell lysates were incubated with anti-FLAG antibody conjugated beads (Sigma) or anti-HA conjugated beads (ThermoFisher Scientific) at 4°C for 2hrs. Endogenous IPs were achieved by incubating lysate with anti-PP5 antibody (Cell Signaling), anti-FADD antibody (Cell Signaling), or anti-RIPK1 antibody (Cell Signaling) overnight followed by protein G agarose (Invitrogen) at 4°C for 2hrs. Immunopellets were washed 4 times with fresh lysis buffer (20 mM Tris-HCl (pH 7.4), 100 mM NaCl, 1 mM MgCl₂, 0.1% NP40, protease inhibitor cocktail (Roche), and PhosSTOP (Roche)) and eluted in 5× Laemmli buffer. Precipitated proteins were separated by SDS-PAGE and transferred to nitrocellulose membranes. Co-immunoprecipitated proteins or proteins from cell lysate were detected with antibodies recognizing FLAG, 6x-His (ThermoFisher Scientific), GAPDH (ENZO Life Sciences), Cdc37 (StressMarq), GR, phospho-GR (S211), PP5, caspase-3, cleaved caspase-3, caspase-8, cleaved caspase-8, cleaved caspase-7, cleaved-PARP, phospho-RIPK1 (S166), phospho-FADD (S194), PP2A-C, VHL (Cell Signaling), phospho-RIPK1 (S161) (Invitrogen), PP5 and phospho-Cdc37 (S13) (Abcam). Secondary antibodies raised against mouse and rabbit (Cell Signaling) were used (See [key resources table](#)).

Bacterial expression and protein purification of PP5

Human *PPP5c* was cloned into pGEX6P1 with an N-terminal GST tag and C-terminal His₆ tag. Transformed cells were grown at 37°C in LB with 100 mg/L ampicillin until OD₆₀₀ = 0.6 and induced with 1 mM IPTG. Cells were harvested by centrifugation and lysed by

sonication in lysis buffer (50 mM HEPES (pH 8.0), 150 mM NaCl, 0.5 mM TCEP and EDTA-free protease inhibitor cocktail tablet (Roche)). Lysate was incubated with talon resin (Takara Bio) for 1 h at 4°C. The resin was washed three times with lysis buffer and PP5 was eluted with lysis buffer containing 250 mM imidazole. Precision protease was added to the elution overnight to cleave the GST tag and the sample was then mixed with Glutathione Sepharose resin (Cytiva) to remove the free GST and un-cleaved protein. The sample was applied to a Superdex S75 16/60 size exclusion column (GE Healthcare) and eluted in 100 mM NaCl, 20 mM HEPES pH 8, 0.2 mM TCEP.

Cell viability assay

Renal cancer cell lines 786-O, Caki-2, Caki-1, and A498 as well as the normal renal cell line HK-2 were plated at 10,000 cells per well in 96-well plates. Cells were treated with different amounts of inhibitors (P075, P059, P058, P13, P053) and DMSO was used as control (0 μ M). After 24 or 48hrs, cell viability assay was performed using the Quick Cell Proliferation Kit Plus (BioVision) according to the manufacturer's protocol. The absorbance at 450 nm was measured on a Tecan Infinite M200 Pro and proliferation rate was calculated.

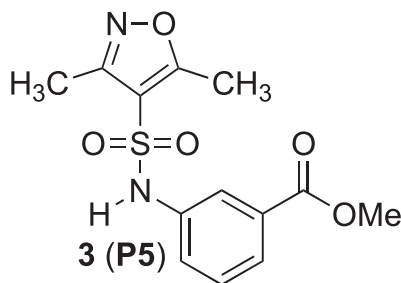
In silico docking

Virtual high throughput docking simulations were carried out using Dockblaster³⁰ with the Zinc library of drug like compounds (~3.7 million compounds).^{28,29} PDB structures of PP5 (PDB: 3H60 and 3H66) were used as receptor structures. In preparation for docking the water molecules were eliminated, and any missing hydrogens and charges were added to the system to generate the receptor input file. The active site residues of D271, N303, H304, M309 and W386 were chosen to define the active site for docking, as these residues are nearby the active site. Once biological activity of an inhibitor was confirmed, docking was performed again using Autodock Vina⁶⁷ to generate docking poses which were used to guide synthetic efforts. The Autodock docking calculation was carried out using a grid per map with 40 \times 40 \times 40 Å points of (PDB: 3H60) in addition to a grid-point spacing of 0.375 Å, which was centered on the metals in the active site.

Synthesis of small molecules

General experimental information for the synthesis of small molecules

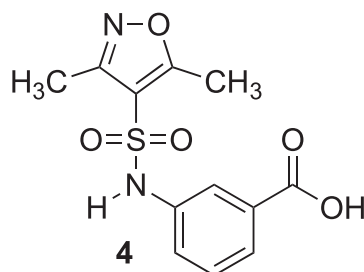
All anhydrous reactions were run under a positive pressure of argon. Dichloromethane (DCM) was dried by passage through an alumina column. 1,2-Dichloroethane (DCE) was freshly distilled from calcium hydride before use. Tetrahydrofuran (THF) was freshly distilled from Na/benzophenone still before use. DMF was distilled from calcium hydride under reduced pressure. Ethyl acetate (EA) and hexanes were purchased from commercial sources and used as received. Silica gel column chromatography was performed using 60 Å silica gel (230–400 mesh). Melting points were obtained on crystalline compounds and are uncorrected. The BODIPY acid **13** was prepared as reported previously.⁵⁸



Methyl 3-aminobenzoate **2** (4.23 g, 28.1 mmol) was dissolved in 52 mL DMF and cooled to 0°C. Pyridine (4.1 mL, 51 mmol) was then added and the mixture stirred for 10 min. 3,5-Dimethyl-isoxazole-4-sulfonyl chloride **1** (5.00 g, 25.5 mmol) was then added in portions over 1 h. The reaction was then allowed to warm to room temperature (RT) and stirred for 16 h. The reaction was quenched by adding 1M HCl until the pH remained below 2 (~60 mL). The reaction mixture was then taken up in EA (400 mL) and washed with 1M HCl (2 \times 200 mL) and brine (2 \times 200 mL). The organic layer was dried (MgSO₄) and concentrated to give a yellow solid. Purification using silica gel chromatography (50% EA/50% hexanes) provided pure **3** (5.65 g, 72%) as a yellow solid.

Methyl *m*-(3,5-dimethyl-4-isoxazolylsulfonylamino)benzoate **3** (P5)

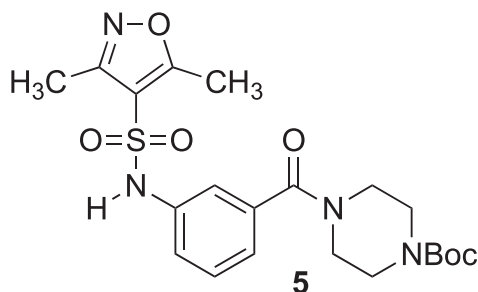
mp = 140–142°C; TLC Rf = 0.45 (50% EA/50% hexanes); IR (ATR) 3226, 2970, 2359, 2341, 1692, 1588, 1339, 1306 cm⁻¹; ¹H NMR (400 MHz, CDCl₃) δ 7.84–7.81 (m, 2H), 7.79 (bs, 1H), 7.43–7.36 (m, 2H), 3.93 (s, 3H), 2.52 (s, 3H), 2.30 (s, 3H); ¹³C NMR (100 MHz, CDCl₃) δ 174.4, 166.6, 157.6, 136.5, 131.5, 129.9, 126.8, 125.7, 122.3, 115.4, 52.8, 12.7, 10.8; HRMS (ESI+) *m/z* calculated (calcd) for C₁₃H₁₄N₂O₅S [M + Na]⁺: 333.0516, found: 333.0515.



Potassium hydroxide (8.5 g, 152 mmol) was dissolved in 40 mL of water and MeOH (160 mL) was added. The ester **3** (**P5**) (5.2 g, 16.9 mmol) was then added and the reaction mixture was stirred for 16 h at RT. The reaction mixture was then quenched by slowly adding 1M HCl until the pH remained below 2 (~180 mL). The methanol was then removed *in vacuo* and the residue was taken up in water (200 mL). This mixture was extracted with EA (3 × 150 mL), and the combined organic extracts were dried (MgSO₄) and concentrated to provide carboxylic acid **4** (4.82 g, 96%) as an off white solid which was used without further purification.

m*-(3,5-Dimethyl-4-isoxazolylsulfonylamino)benzoic acid **4*

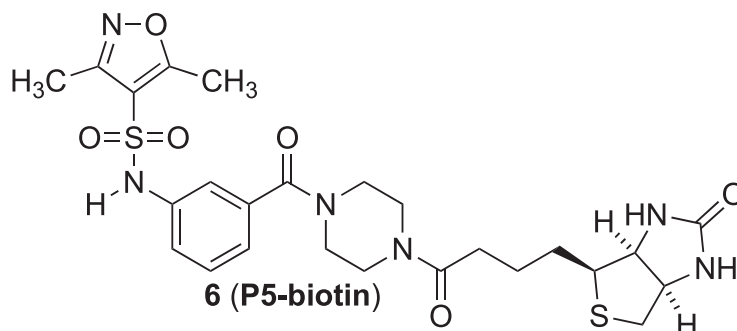
mp = 184–187°C; TLC R_f = 0.51 (100% EA); IR (ATR) 3157, 2980, 2359, 1694, 1590, 1408, 1118 cm⁻¹; ¹H NMR (400 MHz, CD₃OD) δ 7.80–7.78 (m, 2H), 7.42–7.38 (m, 1H), 7.33–7.30 (m, 1H), 2.49 (s, 3H), 2.26 (s, 3H); ¹³C NMR (100 MHz, CD₃OD) δ 175.3, 168.8, 158.9, 138.6, 133.2, 130.6, 127.4, 126.7, 123.1, 116.8, 12.5, 10.7.



Carboxylic acid **4** (1.0 g, 3.37 mmol) was dissolved in 25 mL DMF and EDCI (0.79 g, 5.05 mmol), HOBt (80%, 0.95 g, 6.31 mmol) and diisopropylethylamine (0.88 mL, 5.05 mmol) were added. After aging for 30 min, *tert*-butyl piperazine-1-carboxylate (0.94 g, 5.05 mmol) was then added in one portion. The reaction mixture was stirred at RT for 3 h, and then quenched by the addition of brine (30 mL). The mixture was then taken up in EA (100 mL) and washed with water (2 × 60 mL) and brine (2 × 60 mL). The organic layer was then dried (MgSO₄) and concentrated. Purification of the residue using silica gel chromatography (60% EA/40% hexanes) gave amide **5** as a white solid (1.62 g, 94%).

tert*-Butyl 4-[*m*-(3,5-dimethyl-4-isoxazolylsulfonylamino)benzoyl]-1-piperazine carboxylate **5*

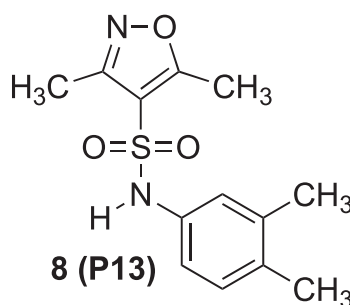
mp = 187–189°C; TLC R_f = 0.61 (80% EA/20% hexanes); IR (ATR) 3080, 2974, 2359, 2341, 1618, 1614, 1165, 1120 cm⁻¹; ¹H NMR (400 MHz, CDCl₃) δ 8.59 (bs, 1H), 7.32–7.30 (m, 2H), 7.15–7.12 (m, 2H), 3.76–3.37 (m, 8H), 2.49 (s, 3H), 2.28 (s, 3H), 1.47 (s, 9H); ¹³C NMR (100 MHz, CDCl₃) δ 173.7, 169.7, 157.6, 154.5, 137.1, 136.2, 129.5, 123.8, 123.3, 121.4, 115.6, 80.6, 47.7, 47.6, 43.5, 42.5, 28.4, 12.6, 10.8.



The Boc protected amine **5** (0.95 g, 20.43 mmol) was dissolved in 1:1 DCM:TFA (60 mL) and stirred for 1 h. The solvent was then evaporated, and the crude TFA salt was used in the next step without further purification. Biotin (1.01 g, 2.19 mmol), EDCI (0.51 g, 3.3 mmol), HOBT (0.62 g, 4.1 mmol) were dissolved in 20 mL of DMF and diisopropylethylamine (0.77 mL, 4.4 mmol) was then added. After stirring for 10 min the crude TFA salt (0.80 g) was then added to the reaction mixture in portions. The reaction was then stirred for 16 h at RT. The reaction mixture was then taken up in brine (30 mL) and extracted with EA (3 × 30 mL). The combined organic layers were washed with water (2 × 30 mL) and brine (2 × 30 mL), dried (MgSO₄) and concentrated. Purification using silica gel chromatography (5% MeOH/95% DCM) gave the biotin-P5 **6** as a white solid (0.53 g, 40%).

N-[3-(4-(4-[(3aS,4S,6aR)-2-Oxo-hexahydro-1H-thieno[3,4-d]imidazol-4-yl]butanoyl) piperazine-1-carbonyl)phenyl]-3,5-dimethyl-1,2-oxazole-4-sulfonamide **6 (biotin-P5)**

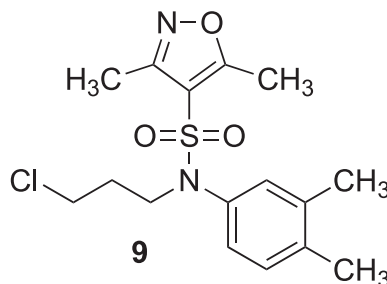
TLC Rf = 0.40 (30% EA/70% toluene); IR (ATR) 3083, 2978, 2359, 2341, 1686, 1614, 1406, 1120 cm⁻¹; ¹H NMR (400 MHz, CDCl₃) δ 7.43 (t, *J* = 7.9 Hz, 1H), 7.27–7.24 (m, 2H), 7.19–7.18 (m, 1H), 4.49 (dd, *J* = 7.8, 4.7 Hz, 1H), 4.31 (dd, *J* = 7.8, 4.4 Hz, 1H), 3.67–3.37 (m, 8H), 3.24–3.20 (m, 3H), 2.93 (dd, *J* = 12.7, 4.9 Hz, 1H), 2.70 (d, *J* = 12.7 Hz, 1H), 2.48–2.47 (m, 5H), 2.25 (s, 3H), 1.78–1.57 (m, 4H), 1.51–1.46 (m, 2H); ¹³C NMR (100 MHz, CDCl₃) δ 175.2, 174.2, 171.5, 166.0, 158.9, 138.7, 137.7, 131.0, 125.0, 124.5, 116.9, 63.3, 61.6, 57.0, 46.4, 42.8, 42.6, 41.0, 33.6, 29.8, 29.5, 26.2, 12.6, 10.8; HRMS (ESI+) *m/z* calcd for C₂₆H₃₄N₆O₆S₂ [M + Na]⁺: 613.1879, found: 613.1872.



3,4-Dimethylaniline **7** (1.36 g, 11.2 mmol) was dissolved in 20 mL DMF and cooled to 0°C. Pyridine (1.7 mL, 20.4 mmol) was then added and the mixture stirred for 10 min 3,5-Dimethyl-isoxazole-4-sulfonyl chloride **1** (2.00 g, 10.2 mmol) was then added in portions over 1 h. The reaction was then allowed to warm to RT and stirred for 16 h. The reaction was quenched by adding 1M HCl until the pH remained below 2 (~25 mL). The reaction mixture was then taken up in EA (80 mL) and washed with 1M HCl (2 × 50 mL) and brine (2 × 50 mL). The organic layer was then dried with MgSO₄. Filtration and evaporation of solvent yielded a red-brown solid which was further purified using silica gel chromatography (40% EA/60% hexanes) to provide sulfonamide **8** as a beige solid (2.04 g, 73%).

(3,5-Dimethyl-4-isoxazolylsulfonyl)(3,4-xylyl)amine **8 (P13)**

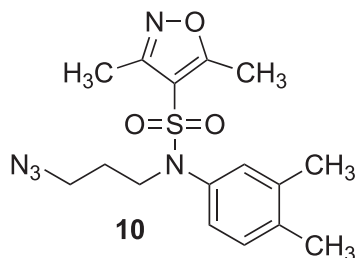
mp = 90–92°C; TLC Rf = 0.48 (50% EA/50% hexanes); IR (ATR) 3250, 2920, 1591, 1327, 1118 cm⁻¹; ¹H NMR (400 MHz, CDCl₃) δ 7.06–7.01 (m, 2H), 6.87–6.86 (m, 1H), 6.81 (dd, *J* = 8.0, 2.4 Hz, 1H), 2.42 (s, 3H), 2.27 (s, 3H), 2.20 (s, 3H), 2.19 (s, 3H); ¹³C NMR (100 MHz, CDCl₃) δ 174, 157.8, 138.2, 135.3, 133, 130.6, 124.4, 120.5, 115.5, 19.8, 19.3, 12.6, 10.9. HRMS (ESI+) *m/z* calcd for C₁₃H₁₆N₂O₃S [M + H]⁺: 281.0954, found: 281.0955.



The sulfonamide **8** (**P13**) (1.80 g, 6.42 mmol) and K₂CO₃ (1.95 g, 14.12 mmol) were suspended in 22 mL DMF and stirred for 15 min at RT. 3-Chloropropyl *p*-toluenesulfonate (2.39 g, 9.63 mmol) was then added and the reaction was heated to 80°C (oil bath temperature). After 20 h, the reaction mixture was allowed to cool to RT and 30 mL water was added. The reaction mixture was then extracted with EA (3 × 30 mL). The combined organic layers were washed with brine (100 mL), dried with MgSO₄ and filtered. After evaporating the solvent, the residue was purified using silica gel chromatography (5% EA/95% hexanes) to provide alkyl chloride **9** as a pale yellow solid (1.89 g, 83%).

(3-Chloropropyl)(3,5-dimethyl-4-isoxazolylsulfonyl)(3,4-xylyl)amine 9

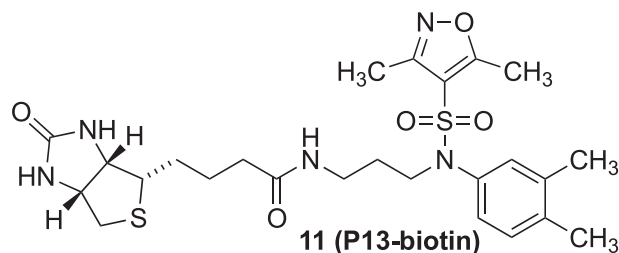
mp = 90–93°C; TLC Rf = 0.68 (30% EA/70% hexanes); IR (ATR) 2923, 2358, 1587, 1346, 1121, 689 cm⁻¹; ¹H NMR (400 MHz, CDCl₃) δ 7.09 (d, *J* = 8.0 Hz, 1H), 6.94 (d, *J* = 2.0 Hz, 1H), 6.85 (dd, *J* = 8.4, 2.4 Hz, 1H), 3.75 (t, *J* = 6.7 Hz, 2H), 3.57 (t, *J* = 6.3 Hz, 2H), 2.27 (s, 3H), 2.26 (s, 3H), 2.23 (s, 3H), 1.96–1.90 (m, 2H); ¹³C NMR (100 MHz, CDCl₃) δ 173.6, 158, 138.1, 137.5, 135.5, 130.5, 129.9, 125.6, 114.8, 47.7, 41.6, 31.2, 19.8, 19.4, 12.5, 11.0.



The alkyl chloride **19** (0.85 g, 2.2 mmol) was dissolved in 7 mL of DMF. Sodium azide (0.4 g, 6.6 mmol) was then added and the reaction mixture was heated to 80°C (oil bath temperature). After 16 h the mixture was allowed to cool to RT and 30 mL water was added. The reaction mixture was then extracted with EA (2 × 50 mL). The combined organic layers were washed with brine (100 mL), dried with MgSO₄, filtered and concentrated *in vacuo*. This gave azide **10** as a yellow foam (0.80 g, 92%) which was used without further purification.

(3-Azidopropyl)(3,5-dimethyl-4-isoxazolylsulfonyl)(3,4-xylyl)amine 1

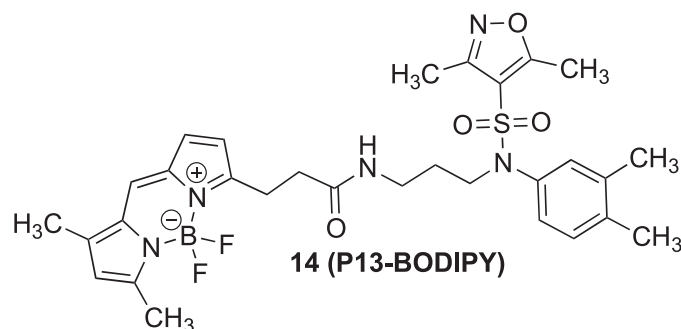
TLC Rf = 0.46 (30% EA/70% hexanes); IR (ATR) 2938, 2358, 2096, 1587, 1346, 1180 cm⁻¹; ¹H NMR (400 MHz, CDCl₃) δ 7.09 (d, *J* = 8.0 Hz, 1H), 6.93 (d, *J* = 2.1 Hz, 1H), 6.83 (dd, *J* = 10.2, 2.2 Hz, 1H), 3.68 (t, *J* = 6.6 Hz, 2H), 3.38 (t, *J* = 6.6 Hz, 2H), 2.25–2.24 (m, 6H), 2.22 (s, 3H), 2.09 (s, 3H), 1.79–1.72 (m, 2H); ¹³C NMR (100 MHz, CDCl₃) δ 173.6, 158, 138.2, 137.6, 135.4, 130.5, 129.8, 125.6, 114.9, 48.4, 47.6, 27.8, 19.7, 19.4, 12.5, 11.0.



The azide **10** (1.00 g, 2.75 mmol) was dissolved in 20 mL of THF. Water (4 mL) was then added followed by triphenyl phosphine (0.79 g, 3.03 mmol). After 16 h at RT the solvent was evaporated and excess triphenyl phosphine was removed by passing the residue through a short plug of silica gel (20% EA/80% hexanes). This provided the amine product containing some triphenyl phosphine oxide, which was used without further purification. Biotin (1.32 g, 5.4 mmol), EDCI (0.84 g, 5.4 mmol) and diisopropylethylamine (0.95 mL, 5.4 mmol) were dissolved in 27 mL of DMF and stirred for 10 min. The crude amine (0.91 g) was then added to the reaction mixture. After 16 h at RT brine (30 mL) was added and the reaction mixture was extracted with EA (3 × 30 mL). The combined organic layers washed with water (1 × 30 mL) and brine (2 × 30 mL), dried (MgSO₄), filtered and concentrated. The residue was purified using silica gel chromatography (15% MeOH/85% DCM) to provide the amide **11** (biotin-P13) as a waxy yellow solid (0.30 g, 20%).

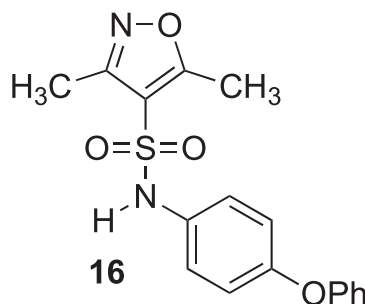
4-[(3aS,4S,6aR)-2-Oxo-hexahydro-1H-thieno[3,4-d]imidazol-4-yl]-N-(3-[N-(3,4-dimethylphenyl)3,5-dimethyl-1,2-oxazole-4-sulfonamido]propyl)butanamide 11 (biotin-P13)

TLC Rf = 0.32 (10% MeOH/90% DCM); IR (ATR) 3208, 2923, 2359, 2341, 1696, 1641, 1342, 1116, 688 cm⁻¹; ¹H NMR (400 MHz, CDCl₃) δ 7.14 (d, *J* = 8.4 Hz, 1H), 7.00–6.99 (m, 1H), 6.92 (dd, *J* = 8.0, 2.2 Hz, 1H), 6.47 (bs, 1H), 5.55 (bs, 1H), 5.23 (bs, 1H), 4.42–4.39 (m, 1H), 4.23–4.20 (m, 1H), 3.61 (t, *J* = 5.1 Hz, 2H), 3.17–3.12 (m, 3H), 2.87 (dd, *J* = 12.7, 4.9 Hz, 1H), 2.63 (d, *J* = 12.7 Hz, 1H), 2.27 (s, 3H), 2.25 (s, 3H), 2.21 (s, 3H), 2.08 (t, *J* = 7.4 Hz, 3H), 1.99 (s, 3H), 1.71–1.48 (m, 6H), 1.39–1.31 (m, 2H); ¹³C NMR (100 MHz, CDCl₃) δ 174.7, 173.7–9, 163.9, 158.8, 138.8, 138.3, 136.5, 131.0, 130.7, 127.0, 115.5, 62.3, 60.7, 56.3, 48.7, 41.1, 36.9, 36.3, 29, 28.9, 28.8, 26.4, 19.7, 19.4, 12.8, 11.1; HRMS (ESI+) *m/z* calcd for C₂₆H₃₇N₅O₅S₂ [M + Na]⁺: 586.2134, found: 586.2119.



The azide **12** (1.00 g, 2.75 mmol) was dissolved in 20 mL of THF. Water (4 mL) was then added followed by triphenyl phosphine (0.79 g, 3.03 mmol). After 16 h at RT the solvent was evaporated and excess triphenyl phosphine was removed by passing the residue through a short plug of silica gel (20% EA/80% hexanes). This provided the amine product containing some triphenyl phosphine oxide, which was used without further purification. 4,4-Difluoro-5,7-dimethyl-4-bora-3a,4a-diaza-s-indacene-3-propionic acid (BODIPY Acid **13**) (0.043 g, 0.148 mmol) was dissolved in DMF (2 mL) and HATU (0.112 g, 0.296 mmol) was added. After 5 min the amine from the previous step (0.050 g, 0.148 mmol) was added followed by addition of diisopropylethylamine (0.05 mL, 0.296 mmol). The reaction mixture was stirred at RT for 16 h, and was then quenched by addition of sat. NH_4Cl (10 mL) and then extracted with DCM (3 \times 5 mL). The combined organic layers washed with water (1 \times 5 mL) and brine (2 \times 5 mL), dried (MgSO_4), filtered and concentrated. Purification of the residue by column chromatography (30% DCM/EA) yielded the amide **14** (BODIPY-P13) as dark red crystals (0.078 g, 87%).

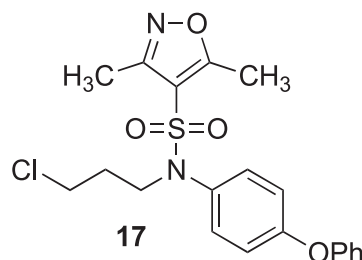
12-[2-((3-[N-(3,4-Dimethylphenyl)3,5-dimethyl-1,2-oxazole-4-sulfonyl]propyl) carbamoyl)ethyl]-2,2-difluoro-4,6-dimethyl-1 λ^5 ,3-diaza-2-boratricyclo[7.3.0.0³,7]dodeca 1(12), 4,6,8,10-pentaen-1-ylidene-2-ylidene 14 (BODIPY-P13)
mp = 175–177°C; TLC R_f = 0.68 (30% DCM/EA); ^1H NMR (400 MHz, CDCl_3) δ 7.08 (s, 1H), 7.06 (s, 1H), 6.91 (s, 1H), 6.85 (d, J = 3.7 Hz, 1H), 6.81 (d, J = 7.9 Hz, 1H), 6.27 (d, J = 3.7 Hz, 1H), 6.13 (s, 1H), 5.99 (bs, 1H), 3.57 (t, J = 6.4 Hz, 2H), 3.33–3.24 (m, 4H), 2.62 (t, J = 7.5 Hz, 2H), 2.56 (s, 3H), 2.26 (s, 3H), 2.24 (s, 6H), 2.22 (s, 3H), 2.06 (s, 3H), 1.61–1.54 (m, 2H); ^{13}C NMR (100 MHz, CDCl_3) δ 173.4, 171.8, 160.3, 158, 157.4, 143.9, 138, 137.4, 135.3, 135.1, 133.3, 130.4, 129.9, 128.1, 125.7, 123.8, 120.4, 117.4, 115, 47.8, 36, 35.9, 27.8, 24.8, 19.8, 19.4, 14.9, 12.5, 11.3, 11.0.



4-Phenoxy aniline **15** (1.00 g, 5.4 mmol) was dissolved in 15 mL DMF and cooled to 0°C. Pyridine (0.90 mL, 10.8 mmol) was then added. After 10 min, 3,5-dimethyl-isoxazole-4-sulfonyl chloride **1** (1.16 g, 5.94 mmol) was added in portions over 15 min. After the addition was complete the ice bath was removed and the reaction mixture was allowed to warm to RT. After 16 h the reaction was quenched by adding 1M HCl until the pH remained below 2 (~15 mL). The reaction mixture was then extracted with EA (2 \times 20 mL). The combined organic layers were washed with 1M HCl (2 \times 20 mL) and brine (2 \times 20 mL), dried (MgSO_4) and concentrated. The residue was purified using silica gel chromatography (40% EA/60% hexanes) that provided sulfonamide **16** as an off-white powder (1.58 g, 91%).

(3,5-Dimethyl-4-isoxazolylsulfonyl)(p-phenoxyphenyl)amine 16 (P052)

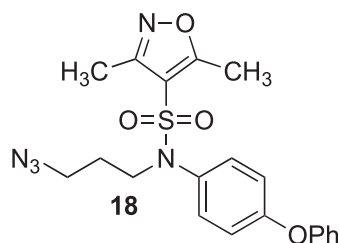
mp = 106–109°C; TLC R_f = 0.30 (50% EA/hexanes); ^1H NMR (400 MHz, CDCl_3) δ 7.35 (t, J = 7.5 Hz, 2H), 7.14 (t, J = 7.4 Hz, 1H), 7.05 (d, J = 7.4, 2H), 6.98 (d, J = 8.3 Hz, 2H), 6.93 (d, J = 9.0 Hz, 2H), 6.44 (bs, 1H), 2.42 (s, 3H), 2.29 (s, 3H); ^{13}C NMR (100 MHz, CDCl_3) δ 173.9, 157.6, 156.6, 156.5, 129.9, 129.8, 126, 123.9, 119.4, 119.2, 115.2, 12.5, 10.8; Anal. Calcd for $\text{C}_{17}\text{H}_{16}\text{N}_2\text{O}_4\text{S}$: C, 59.29; H, 4.68; N, 8.13. Found: C, 59.23; H, 4.78; N, 8.17.



The sulfonamide **16** (0.2 g, 0.58 mmol) and K_2CO_3 (0.24 g, 1.74 mmol) were suspended in 25 mL of MeCN and stirred for 15 min at rt. 3-Chloropropyl *p*-toluenesulfonate (0.29 g, 1.16 mmol (prepared as described in⁵⁹) was then added and the reaction mixture warmed to reflux. After 20 h the reaction was allowed to cool to RT and 30 mL water was added. The reaction mixture was extracted with EA (3 × 30 mL). The combined organic extracts were washed with brine (100 mL), dried ($MgSO_4$), filtered and concentrated. Purification of the residue using silica gel chromatography (50% EA/50% hexanes) gave alkyl chloride **17** as an off-white powder (0.190 g, 77%).

(3-Chloropropyl)(3,5-dimethyl-4-isoxazolylsulfonyl)(p-phenoxyphenyl)amine 17 (P059)

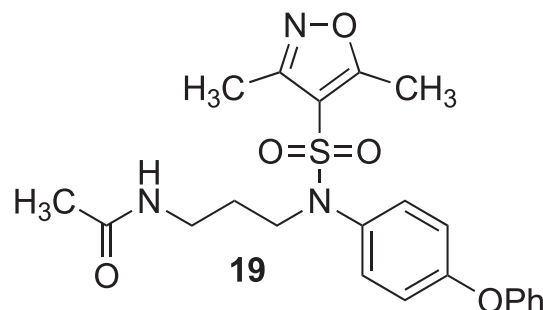
mp = 95–98°C; TLC R_f = 0.21 (50% DCM/hexanes); 1H NMR (400 MHz, $CDCl_3$) δ 7.38 (t, J = 7.8 Hz, 2H), 7.17 (t, J = 7.4 Hz, 1H), 7.11 (d, J = 8.8 Hz, 2H), 7.01 (d, J = 7.8 Hz, 2H), 6.96 (d, J = 8.8 Hz, 1H), 3.77 (t, J = 6.8 Hz, 2H), 3.59 (t, J = 6.3 Hz, 2H), 2.32 (s, 3H), 2.15 (s, 3H), 2.00–1.94 (m, 2H); ^{13}C NMR (100 MHz, $CDCl_3$) δ 173.7, 157.9, 156, 132.5, 130.2, 130, 124.3, 119.5, 118.9, 114.7, 47.9, 41.5, 31.3, 12.5, 11.0; Anal. Calcd for $C_{20}H_{21}ClN_2O_4S$: C, 57.07; H, 5.03; N, 6.66. Found: C, 56.98; H, 5.10; N, 6.60.



The alkyl chloride **17** (0.100 g, 0.24 mmol) was dissolved in 1 mL of DMF. Sodium azide (0.050 g, 0.71 mmol) was then added and the reaction mixture was warmed to 80°C. After 16 h the reaction mixture was allowed to cool to RT and 10 mL water was added. The reaction mixture was extracted with EA (3 × 5 mL). The combined organic extracts were washed with brine (10 mL), dried ($MgSO_4$), filtered and concentrated. This provided the azide **18** a tan solid (0.090 g, 87%).

(3-Azidopropyl)(3,5-dimethyl-4-isoxazolylsulfonyl)(p-phenoxyphenyl)amine 18 (P062)

mp = 72–76°C; TLC R_f = 0.63 (30% EA/70% hexanes); IR (ATR) 3076, 2935, 2091, 1585, 1484, 1345 cm^{-1} ; 1H NMR (400 MHz, $CDCl_3$) δ 7.37 (t, J = 7.7 Hz, 2H), 7.17 (t, J = 7.4 Hz, 1H), 7.11 (d, J = 8.8 Hz, 2H), 7.01 (d, J = 8.2 Hz, 2H), 6.97 (d, J = 8.7 Hz, 2H), 3.71 (t, J = 6.7 Hz, 2H), 3.34 (t, J = 6.6 Hz, 2H), 2.31 (s, 3H), 2.15 (s, 3H), 1.79–1.72 (m, 2H); ^{13}C NMR (100 MHz, $CDCl_3$) δ 173.6, 157.9, 157.8, 156, 132.4, 130.2, 130, 124.3, 119.5, 118.9, 114.7, 48.4, 47.8, 27.9, 12.5, 11.0; Anal. Calcd for $C_{20}H_{21}N_5O_4S$: C, 56.19; H, 4.95; N, 16.38. Found: C, 56.15; H, 4.87; N, 16.45.

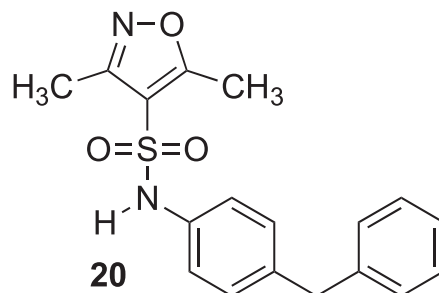


The azide **18** (0.55 g, 1.29 mmol) was dissolved in 10 mL of THF and water (2 mL) was added followed by triphenyl phosphine (0.38 g, 1.42 mmol). After 16 h at RT the solvent was evaporated and the residue was put through a plug of silica gel (20% EA/80% hexanes). This gave the amine product containing small amounts of triphenyl phosphine oxide. This amine (0.05 g, 0.12 mmol) was

dissolved in 0.5 mL of DCM and cooled to 0°C. Pyridine (0.06 mL, 0.07 mmol) was then added, followed by acetic anhydride (0.013 mL, 0.14 mmol). After 3 h at RT 5 mL water was added and the reaction mixture was extracted with DCM (3 × 5 mL). The combined organic extracts were washed with sat. aq. NaHCO₃ (5 mL) and brine (5 mL), dried (MgSO₄), filtered and concentrated. Purification of the residue using silica gel chromatography (10% MeOH/DCM) provided acetamide **19** as a white foam (0.040 g, 73%).

1-(3-[(3,5-Dimethyl-4-isoxazolylsulfonyl)(p-phenoxyphenyl)amino]propylamino)-1-ethanone 19 (P070)

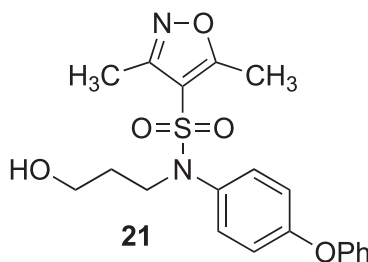
TLC R_f = 0.44 (100% EA); IR (ATR) 3265, 3097, 2936, 1629, 1502, 1343, 1246 cm⁻¹; ¹H NMR (400 MHz, CDCl₃) δ 7.36 (t, *J* = 7.6 Hz, 2H), 7.16 (t, *J* = 7.4 Hz, 1H), 7.36 (d, *J* = 8.8 Hz, 2H), 6.93 (d, *J* = 7.8 Hz, 2H), 6.95 (d, *J* = 8.8 Hz, 1H), 3.67 (t, *J* = 6.3 Hz, 2H), 3.36 (q, *J* = 6.2 Hz, 2H), 2.30 (s, 3H), 2.14 (s, 3H), 1.99 (s, 3H), 1.69–1.62 (m, 2H); ¹³C NMR (100 MHz, CDCl₃) δ 173.5, 170.5, 157.9, 157.7, 156, 132, 130.3, 130, 124.3, 119.6, 118.9, 114.8, 47.9, 36, 27.5, 23.2, 12.5, 11.0; Anal. Calcd for C₂₂H₂₅N₃O₅S: C, 59.58; H, 5.68; N, 9.47. Found: C, 59.63; H, 5.74; N, 9.26.



4-Benzylaniline (0.5 g, 2.73 mmol) was dissolved in 10 mL of DMF and cooled to 0°C. Pyridine (0.44 mL, 5.46 mmol) was then added. After 10 min, 3,5-dimethyl-isoxazole-4-sulfonyl chloride **1** (0.59 g, 3 mmol) was added in portions over 15 min. After 16 h the reaction was quenched by adding 1M HCl until the pH was maintained below 2. The reaction mixture was then taken up in EA (50 mL) and washed with 1M HCl (2 × 20 mL) and brine (2 × 20 mL). The organic layer was then dried (MgSO₄), filtered and concentrated. The residue was purified using silica gel chromatography (10% EA/90% hexanes) to obtain sulfonamide **20** as a light brown foam (0.482 g, 47%).

(3,5-Dimethyl-4-isoxazolylsulfonyl)(p-benzylphenyl)amine 20 (P053)

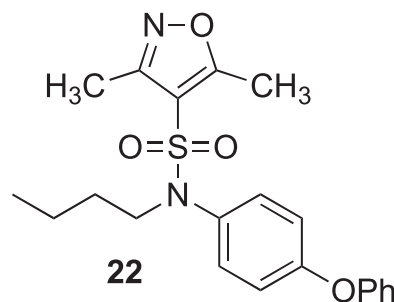
mp = 111–115°C; IR (ATR) 3227, 2951, 1588, 1490, 1337, 1179 cm⁻¹; ¹H NMR (400 MHz, CDCl₃) δ 7.28 (t, *J* = 7.2 Hz, 2H), 7.20 (t, *J* = 7.3 Hz, 1H), 7.14–7.11 (m, 4H), 6.99 (d, *J* = 8.4 Hz, 2H), 6.8 (bs, 1H), 3.94 (s, 2H), 2.39 (s, 3H), 2.25 (s, 3H); ¹³C NMR (100 MHz, CDCl₃) δ 173.9, 157.6, 140.4, 140.1, 133.2, 130, 128.8, 128.6, 126.3, 123.6, 115.3, 41.3, 12.5, 10.7; Anal. Calcd for C₁₈H₁₈N₂O₃S: C, 63.14; H, 5.30; N, 8.18. Found: C, 63.19; H, 5.27; N, 7.99.



The sulfonamide **16** (0.2 g, 0.58 mmol) and K₂CO₃ (0.18 g, 1.28 mmol) were suspended in 2.5 mL of MeCN and stirred for 15 min at RT. 3-Chloropropanol (0.082 g, 0.087 mmol) was then added and the reaction mixture was heated to reflux. After 20 h the reaction mixture was allowed to cool to RT and 30 mL water was added. The reaction mixture was extracted with EA (3 × 10 mL) and the combined organic layers were washed with brine (20 mL), dried (MgSO₄), filtered and concentrated. Purification of the residue using silica gel chromatography (10% EA/90% hexanes) yielded alcohol **21** as a white powder (0.09 g, 39%).

3-[(3,5-Dimethyl-4-isoxazolylsulfonyl)(p-phenoxyphenyl)amino]propanol 21 (P129)

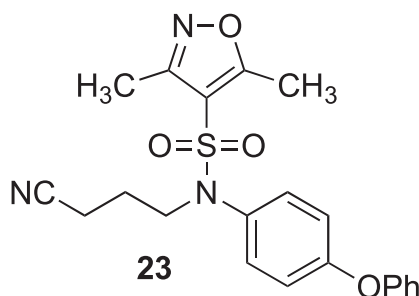
TLC R_f = 0.90 (50% EA/50% hexanes); ¹H NMR (400 MHz, CDCl₃) δ 7.37 (t, *J* = 7.6 Hz, 2H), 7.17 (t, *J* = 7.4 Hz, 1H), 7.12 (d, *J* = 9.1 Hz, 2H), 6.96 (d, *J* = 8.9 Hz, 2H), 3.79–3.75 (m, 4H), 2.33 (s, 3H), 2.16 (s, 3H), 1.72–1.66 (m, 4H); ¹³C NMR (100 MHz, CDCl₃) δ 173.5, 157.8, 157.7, 156.1, 132.4, 130.4, 130, 124.2, 119.5, 118.9, 114.9, 58.8, 47.3, 30.7, 12.6, 11.1; Anal. Calcd for C₂₀H₂₂N₂O₅S: C, 59.69; H, 5.51; N, 6.96. Found: C, 59.61; H, 5.63; N, 6.79.



The sulfonamide **16** (0.2 g, 6.42 mmol) and K_2CO_3 (0.24 g, 1.74 mmol) were dissolved in 20 mL of MeCN and stirred for 15 min at RT. 1-Bromobutane (0.12 mL, 1.16 mmol) was then added and the reaction was heated to 80°C. After 20 h, 30 mL water was added and reaction mixture was extracted with EA (3 × 10 mL). The combined organic layers were washed with brine (50 mL) dried ($MgSO_4$), filtered and concentrated. Purification of the residue with silica gel chromatography (10% EA/90% hexanes) gave sulfonamide **22** as an off-white foam (0.19 g, 83%).

***N*-Butyl(3,5-dimethyl-4-isoxazolylsulfonyl)(*p*-phenoxyphenyl)amine **22** (P058)**

TLC R_f = 0.61 (30% EA/70% hexanes); IR (ATR) 3065, 2951, 2868, 1588, 1503, 1340, 1180 cm^{-1} ; 1H NMR (400 MHz, $CDCl_3$) δ 7.41 (t, J = 7.6 Hz, 2H), 7.19 (t, J = 7.4 Hz, 1H), 7.12 (d, J = 8.9 Hz, 2H), 7.04 (d, J = 7.7 Hz, 2H), 6.98 (d, J = 8.9 Hz, 2H), 3.63 (t, J = 6.8 Hz, 2H), 2.32 (s, 3H), 2.18 (s, 3H), 1.50–1.34 (m, 4H), 0.92 (t, J = 7.2 Hz, 2H); ^{13}C NMR (100 MHz, $CDCl_3$) δ 173.4, 157.9, 157.6, 156.2, 132.6, 130.4, 130, 124.1, 119.4, 118.8, 115.0, 50.1, 30.2, 19.5, 13.5, 12.5, 11.0; Anal. Calcd for $C_{21}H_{24}N_2O_4S$: C, 62.98; H, 6.04; N, 6.99. Found: C, 62.90; H, 6.14; N, 6.85.



Alkyl chloride **17** (0.70 g, 1.67 mmol) was dissolved in DMF (15 mL) and NaCN (0.25 g, 5 mmol) was added. The reaction was then heated to 85°C (oil bath temperature). After 18 h the reaction mixture was allowed to cool to RT and poured into water (50 mL). The resulting mixture was extracted with EA (3 × 30 mL). The combined organic extracts were washed with water (50 mL) and brine (2 × 50 mL), dried ($MgSO_4$), filtered and concentrated. The residue was purified using silica gel chromatography (30% EA/70% hexanes) to obtain nitrile **23** as an off-white crystalline solid (0.62 g, 91%).

***4*-[(3,5-Dimethyl-4-isoxazolylsulfonyl)(*p*-phenoxyphenyl)amino]butyronitrile **23** (P075)**

mp = 78–83°C; TLC R_f = 0.32 (30% EA/70% hexanes); IR (ATR) 3384, 3225, 2938, 2246, 1732, 1586, 1487 cm^{-1} ; 1H NMR (400 MHz, $CDCl_3$) δ 7.41 (t, J = 7.6 Hz, 2H), 7.20 (t, J = 7.4 Hz, 1H), 7.13 (d, J = 8.9 Hz, 2H), 7.04 (d, J = 7.7 Hz, 2H), 6.99 (d, J = 8.9 Hz, 1H), 3.76 (t, J = 6.5 Hz, 2H), 2.51 (t, J = 7.3 Hz, 2H), 2.33 (s, 3H), 2.16 (s, 3H), 1.93–1.87 (m, 2H); ^{13}C NMR (100 MHz, $CDCl_3$) δ 173.8, 158.1, 157.8, 155.9, 132, 130.2, 130, 124.4, 119.7, 118.9, 118.7, 114.5, 49.2, 24.5, 14.4, 12.5, 11.0; Anal. Calcd for $C_{21}H_{21}N_3O_4S$: C, 61.30; H, 5.14; N, 10.21. Found: C, 61.25; H, 5.17; N, 10.06.

Binding measurements and anisotropy

Recombinant PP5-His₆ at the indicated concentrations was incubated on ice in 100 mM NaCl, 20 mM HEPES pH 8.0, 1% glycerol, 0.2 mM tris(2-carboxyethyl)phosphine (TCEP) and 0.5 mM $MnCl_2$ with 10 nM BODIPY-labeled P13 in 2% DMSO for 30 min in opaque black 96 well plates (Corning). Uncalibrated fluorescence anisotropy was then measured using a SpectraMax i3 equipped with fluorescein anisotropy module (Molecular Devices). Curves were fit to a one-site binding equation using GraphPad Prism version 9.5.0. $y = y_0 + A * x / (K_d + x)$ where y is measured uncalibrated anisotropy, y_0 is the y intercept, A is the amplitude of the curve, x is the concentration of PP5 used, and K_d is the measured dissociation constant. Data are presented as mean \pm SEM.

PP5 phosphatase activity and inhibition assay

The phosphatase activity of the recombinant PP5-His₆ was measured using the PiPer Phosphate Assay Kit (Thermo Fisher Scientific) as described in the manufacturer's protocol. Standard curve with linear fit line was created from 0 to 1 nM P_i final concentration reactions. 1 nM of PP5-His₆ was added to each reaction with indicated amounts of custom synthesized substrate phospho-S211-glucocorticoid

receptor (PhosS211-GR) peptide (see [key resources table](#)) as specific substrate (Thermo Fisher Scientific). Reactions were run in triplicate and incubated at 37°C for over 10 min. Reaction was also performed in the presence of different amounts (100–1200 nM) of PP5 inhibitors (P5, P13 and P053). Enzyme kinetics were calculated and plotted using Lineweaver Burk plot and web-based tool (<https://www.aatbio.com/tools/ic50-calculator>) for calculating IC₅₀ and (https://bioinfo-abcc.ncifcrf.gov/IC50_Ki_Converter/index.php) for converting IC₅₀ to K_i values for inhibitors of enzyme activity and ligand binding.⁶⁰

Flow cytometric analysis

Fluorescence-activated cell sorting (FACS) analysis was performed according to the protocol in the Annexin V:FITC kit (Bio-Rad). In brief, cells were plated in 10 cm dish at 0.5×10^6 and incubated at 37°C for 18hrs. Cells were subsequently treated with compound P053 at the indicated concentrations for 18hrs. Cells were trypsinized, collected and washed once with 1 × binding buffer (included in the kit). PI was added, then the cells were immediately run on a Becton Dickinson LSRFortessa instrument (BD Biosciences). Data were analyzed using FlowJo software version 10.7.1 for Windows (BD Biosciences).

Biotin-P5 and biotin-P13 pulldown

HEK293 cells were transiently transfected with PP5-FLAG or active site point mutants and protein lysate extracted. Lysate was incubated with 0.01–10 μM biotin-P5 or biotin P-13 as indicated at 4°C for 1 h then added to streptavidin-conjugated agarose and incubated at 4°C for 1 h. Following three washes with fresh extraction buffer bound proteins were eluted in 5× Laemmli buffer and analyzed by Western blot. Competition experiment with P053 was conducted with protein lysate from untreated 786-O cells. Lysate was incubated with 1 μM biotin-P5 or biotin-P13 for 1 h followed by competition with 1 μM P053 at 4°C for 30 min This was then incubated with streptavidin-conjugated agarose at 4°C for 1 h prior to washing 3× with fresh extraction buffer and elution in 5× Laemmli buffer. Samples were run by SDS PAGE, transferred to nitrocellulose membrane, and analyzed by Western blot.

QUANTIFICATION AND STATISTICAL ANALYSIS

The data presented are representative of three biological replicates, unless otherwise specified. All statistics were performed using GraphPad Prism version 9.5.0 for Windows (GraphPad Software, <https://www.graphpad.com>). Statistical significance was ascertained between individual samples using a parametric unpaired *t*-test. Significance is denoted by asterisks in each figure: **p* < 0.05; ***p* < 0.01; ****p* < 0.001; *****p* < 0.0001. Error bars represent the standard deviation for three independent experiments, unless otherwise indicated.